A micromechanics-based model for visco-super-elastic hydrogel-based nanocomposites

Mahrez Saadedine, Fahmi Zaïri, Nourdine Ouali, Abderrahman Tamoud, Amar Mesbah

Version of Record: https://www.sciencedirect.com/science/article/pii/S0749641921001170
Manuscript_80082f15c3bba85150cc59dfdfb86bd9

A micromechanics-based model for visco-super-elastic hydrogel-based nanocomposites

Mahrez Saadedine[a,b], Fahmi Zaïri[a*], Nourdine Ouali[b], Abderrahman Tamoud[a,b], Amar Mesbah[b]

[a]Lille University, Civil Engineering and geo-Environmental Laboratory (ULR 4515 LGCgE), 59000 Lille, France
[b]University of Sciences and Technology Houari Boumediene, Laboratory of Advanced Mechanics, 16111 Algiers, Algeria

*Corresponding author.
E-mail address: fahmi.zairi@polytech-lille.fr

Abstract

This article presents a micromechanics-based model that constitutively relates internal network physics of hydrogel-based nanocomposites with their visco-super-elastic mechanics. The model is based on the Eshelby inclusion theory combined to the concept of cubic material volume to take into account the effective role of inorganic nanoparticles on the finite-strain response of hydrogels. Dynamic bonds between hydrogel chains and nanoparticles allow to describe the impressive time-dependent properties of hydrogel-based nanocomposites such as rate-dependent extreme stretchability, strong hysteresis upon stretching-retraction and room temperature self-healing facility. The model is compared to a few available experimental data of a variety of hydrogel-nanofiller material systems in terms of stress-strain response till failure, hysteresis, continuous relaxation and self-healing. The effects on the hydrogel behavior of loading conditions (strain rate and strain level) and internal network structures (due to variations in reinforcing elements and cross-linker amounts) are examined. The micromechanical model simulations are found in excellent agreement with experimental observations showing the relevance of the proposed approach. The mechanisms of nanofillers reinforcement and failure are discussed with respect to the model. The room temperature self-healing characteristics of hydrogel systems are discussed in connection to loading history and nanostructure. To further illustrate the model

capabilities, the behavior of hydrogel systems is finally treated under different biaxial loading conditions.

Keywords: Hydrogel-based nanocomposites; Micromechanical modeling; Extreme stretchability; History-dependent effects; Self-healing.

1. Introduction

Amongst the new cohort of advanced materials, hydrogel-based nanocomposites, designed by incorporating nano-sized second phase into hydrogels, have fascinating properties. They have very recently attracted a lot of attention due to the new extraordinary opportunities that such sophisticated and multifunctional materials offer in a wide range of domains including aerospace, 3D printing, waste-water treatment, biomedical engineering (drug delivery and tissue engineering), sensors, actuators and energy storage (Lima-Tenorio et al., 2015; Merino et al., 2015; Bhattacharya and Samanta, 2016; Farahani et al., 2016; Yang et al., 2016; Thakur et al., 2017a, 2017b; Zhai et al., 2017; Liu et al., 2019; Deng et al., 2019; Guo et al., 2019; Xu et al., 2019; Zhang et al., 2019).

While traditional (organically crosslinked) hydrogels have poor mechanical performances (e.g. low fracture toughness and limited ductility), this new class of nanocomposites is extremely resilient and extremely stretchable with an elongation than can exceed 3000%. Very recent studies have illustrated impressive improvements of mechanical properties, in addition to extreme stretchability, such as high toughness and high mechanical strength (Sun et al., 2012; Shi et al., 2015; Chen et al., 2017; Liu et al., 2019). The reinforcing effect of nanoparticles is attributed to several factors such as hydrogel matrix properties, nature (and amount) of nanoparticles and strength of interactions. Nanofillers considerably improve the structural stability of the hydrogels due to the occurrence of multiple specific interactions between the polar surface of the charges and hydrophilic chains such as hydrogen bonds, van

der Waals interactions and electrostatic interactions, to achieve better chemical, electrical, mechanical and biological properties (Sarvestani et al., 2008; Schexnailder and Schmidt, 2009; Kumar et al., 2014). These smart and adaptive materials combine the advantage of the nano-scale reinforcement and the multiphysics (chemical, physical, mechanical and biological) properties of hydrogels including biocompatibility (along with some similarities to biological tissues), stimulating responsiveness, adsorption performance and facile room temperature self-healing (by restoring initial microstructure and mechanical strength).

Whereas considerable efforts have been devoted to elaboration and characterization of hydrogel-filler material systems, the mechanisms of nanofillers reinforcement remain largely misunderstood. Behind the basic inelastic features illustrated in Fig. 1, a better understanding of the structure-property relationship for such new material systems is of prime importance in order to provide detailed information for their reliable design considering a rigorous set of their various specific characteristics: extreme stretchability and self-healing facility along with a strong viscous consistency. As a meaningful prerequisite of advanced applications of such new materials, the formulation of constitutive models is needed. Such tools would provide a better understanding of the separate and synergistic effects of key factors that govern the impressive improvements of mechanical properties. An exhaustive literature survey shows that the constitutive modeling of hydrogels is rare (Long et al., 2014; Guo et al., 2016; Liu et al., 2016; Wang and Gao, 2016; Mao et al., 2107; Shao et al., 2017; Wang et al., 2017; Vernerey et al., 2017, 2018; Vernerey, 2018; Yu et al., 2018; Kulcu, 2019; Morovati and Dargazany, 2019; Drozdov and Christiansen, 2018, 2020; Lin et al., 2020; Zhu and Zhong, 2020; Xiao et al., 2021). More specifically Morovati and Dargazany (2019) proposed a constitutive model based on the network decomposition along with the detachment mechanism to capture the stress-softening in double network hydrogels. Liu et al. (2016), Kulcu (2019) and Xiao et al. (2021) proposed also inelastic constitutive models for

double network hydrogels while Wang and Gao (2016) and Wang et al. (2017) paid attention to the networks crosslinked by nanoparticles. The strong viscous consistency of hydrogels may be represented by using either phenomenological or physically-based approaches. The latter seems more attractive to provide a proper description of the underlying microstructure phenomena in the aim of controlling them (Dargazany et al., 2014; Li et al., 2016; Yang and Li, 2016; Guo et al., 2018; Zhou et al., 2018; Mahjoubi et al., 2019; Xiang et al., 2019; Guo and Zaïri, 2020, 2021). For example, Mao et al. (2017) developed a constitutive model to describe inelastic behavior and stress-softening in double network hydrogels in which the inelastic damage caused by the rupture of ionic bonds is introduced. The self-healing behavior is also an important feature to control by tailoring the microstructure. Intensive efforts have been done to the thermally-induced strain recovery prediction of more conventional amorphous networks (Su and Peng, 2018; Shen et al., 2019; Cherief et al., 2020; Dai et al., 2020) in relation to previous thermo-mechanical history and heating conditions in terms of recovery temperature and heating rate. Actually, hydrogels are room-temperature self-healable materials and this feature has been considered in a very few constitutive models (Long et al., 2014; Vernerey et al., 2017; Wang et al., 2017; Yu et al., 2018; Lin et al., 2020). Long et al. (2014) developed a rate-dependent phenomenological model for dual cross-linked self-healing hydrogels. Vernerey et al. (2017) provided latter a more direct connection between single chain and macroscopic mechanics. Wang et al. (2017) developed a polymer-network based theory to capture the response of self-healable nanocomposite hydrogels taking into account the particle concentration and chain length distribution. However, the chain-particle interaction has been highly simplified. Lu et al. (2020) and Lin et al. (2020) developed constitutive models, based on the eight-chain model and on a Neo-Hookean formulation, respectively, in which association/dissociation of chains were incorporated to capture the recovery behavior of different hydrogel types. The constitutive models are able to

describe the rate-dependent tensile response but the presence of particles is not taken into account.

Despite the important advance accomplished by these models, they cannot connect the nanostructure to the overall recovery behavior of hydrogel-based nanocomposites. A rigorous constitutive representation of the nanofiller-hydrogel material system, including explicit active interactions between nanfillers and hydrogel matrix, would allow to propose physically consistent explanations of the reinforcement mechanisms in connection to the nonlinear material response (Zaïri et al., 2011) and the room-temperature self-healing facility. In this regards, only micromechanics-based approaches allow to propose a framework avoiding (or at least limiting) the arbitrary inclusion of heuristic parameters. Such a development would offer a way to gain a better understanding of the reinforcing effect of nanoparticles on the overall properties and to provide detailed information for their design. A constitutive representation that considers as well history-dependent effects and local matrix-nanoparticle interaction has not yet been developed.

The objective of this study is to constitutively correlate the behavior of visco-super-elastic hydrogel-based nanocomposites to their internal network structures in terms of hydrogel matrix and inorganic nanoparticles properties. We present a model based on the Eshelby inclusion theory and the micromechanics framework using the concept of cubic material volume to account for the effective role of nanoparticles on the nonlinear and finite-strain macro-behavior of hydrogel-based nanocomposites. The hydrogel-nanofiller material system is representatively regarded as a cubic unit cell containing nine particles. A central nanoparticle connects eight nanoparticles placed at the cube vertices via a number of hydrogel chains. The model explicitly considers the chains network with dynamic reversible detachable/re-attachable mechanisms of bonds to coherently capture the rate-dependent extreme stretchability and some inelastic features including strong hysteresis upon stretching-

retraction and continuous relaxation. A quantitative evaluation of our model is presented by comparisons to a few available experimental data of a variety of hydrogel-nanofiller material systems. The model is used to discuss some important aspects of the mechanisms of nanofillers reinforcement, failure and room temperature self-healing facility.

The paper is organized as follows. The micromechanical model is presented in Section 2. Section 3 presents and discusses the model results especially regarding the reinforcing effect of inorganic nanoparticles on the visco-super-elastic response of hydrogels. Concluding remarks are finally given in Section 4.

The following notation is used throughout the text. Tensors and vectors are denoted by normal boldfaced letters and italicized boldfaced letters, respectively, while scalars and individual components of vectors and tensors are denoted by normal italicized letters.

2. Model

2.1. Cubic material volume

When nanoparticles are embedded into a hydrogel medium, the nano-sized discrete second phase acts as anchoring (crosslinking) points for hydrogel chains and strengthens the chains network (Haraguchi et al., 2002; Liu et al., 2019). A multiscale approach starting from the nanostructure is then required to represent the material system. Fig. 2 presents the representative volume element used to derive the model. It arises from the eight-chain cubic material volume of Arruda and Boyce (1993) in which nine nanoparticles are inserted. A central nanoparticle P_0 connects eight nanoparticles (P_1 to P_8) placed at the cube vertices via the eight chains. The hydrogel chains network will be characterized by the mean number of segments in a chain N (mean chain length) and the mean chain density n.

The macroscopic free energy $\bar{\psi}$ from which the stress-strain relationship is obtained may be expressed as a function of the chain free energy ψ_{chain} and the free energy of the nanoparticles ψ_p:

$$\bar{\psi} = \frac{8(b-2r)}{V}\psi_{chain} + \phi\psi_p \tag{1}$$

where b is the center-to-center distance between the central nanoparticle and a neighboring nanoparticle, r is the nanoparticle radius, V is the cubic unit cell volume and ϕ is the volume fraction of nanoparticles.

The quantity ψ_{chain} being an energy density per unit chain length, it may be expressed as a function of the strain energy density per unit volume of the hydrogel matrix ψ_m:

$$\psi_{chain} = \frac{V}{8b}\psi_m \tag{2}$$

Eq. (1) can be re-written as follows:

$$\bar{\psi} = (1-2\rho)\psi_m + \phi\psi_p \tag{3}$$

with $\rho = r/b$.

With increasing amount of nanoparticles, the distance between them decreases. The volume fraction of nanoparticles ϕ is defined as the ratio between the volume of domains Ω_p occupied by the nanoparticles in the cubic unit cell and the total volume V. Since each of the eight nanoparticles P_1 to P_8 occupies a volume of $1/8V_p$ and the central nanoparticle P_0 occupies a volume of V_p, the volume fraction of nanoparticles is given by:

$$\phi = \frac{2V_p}{a^3} = \sqrt{3}\pi\rho^3 \tag{4}$$

where $V_p = 4/3\pi r^3$ is the nanoparticle volume and $a = 2b/\sqrt{3}$ is the cube length.

2.2. Constitutive equations for the two phases

The proposed multiscale model satisfies the continuum mechanics rules for which the deformation gradient tensor $\mathbf{F}$ is a key quantity to define the kinematics of a continuum body with $J=\det(\mathbf{F})$ the Jacobian. Let us define the tensors $\bar{\mathbf{F}}$, $\mathbf{F}_m$ and $\mathbf{F}_p$ the deformation gradients of the hydrogel-nanofiller material system, of the hydrogel matrix and of the nanoparticles, respectively. Each constitutive phase is supposed to be an isotropic and homogeneous medium with the stiffness tensors $\mathbf{K}_m$ and $\mathbf{K}_p$ defined with their respective shear moduli $\mu_m = nk_{\mathrm{B}}T$ (k_{B} is the Boltzmann's constant and T is the absolute temperature) and μ_p, and their respective bulk moduli K_m and K_p.

2.2.1. Hydrogel matrix

As shown in Fig. 2, the chain end-to-end vector $\boldsymbol{c}$ is defined, in the Cartesian coordinate system, by:

$$\boldsymbol{c} = \frac{b-2r}{\sqrt{3}}\left(\lambda_{m\_1}\boldsymbol{x} + \lambda_{m\_2}\boldsymbol{y} + \lambda_{m\_3}\boldsymbol{z}\right) \tag{5}$$

where λ_{m_1}, λ_{m_2} and λ_{m_3} are the principal stretches of the hydrogel matrix.

The vector $\boldsymbol{c}$ may be also defined as follows:

$$\boldsymbol{c} = \boldsymbol{b} - 2\boldsymbol{r} \tag{6}$$

in which $\boldsymbol{b}$ and $\boldsymbol{r}$ are vectors given, in the Cartesian coordinate system, by:

$$\boldsymbol{b} = \frac{b}{\sqrt{3}}\left(\bar{\lambda}_1\boldsymbol{x} + \bar{\lambda}_2\boldsymbol{y} + \bar{\lambda}_3\boldsymbol{z}\right) \text{ and } \boldsymbol{r} = \frac{r}{\sqrt{3}}\left(\lambda_{p\_1}\boldsymbol{x} + \lambda_{p\_2}\boldsymbol{y} + \lambda_{p\_3}\boldsymbol{z}\right) \tag{7}$$

where $\bar{\lambda}_1$, $\bar{\lambda}_2$ and $\bar{\lambda}_3$ are the principal stretches applied at the macro-level and, λ_{p_1}, λ_{p_2} and λ_{p_3} are the principal stretches of the nanoparticles $\mathbf{F}_p$.

Combining Eqs. (5), (6) and (7), the micro-macro transition is realized. The obtained deformation gradient tensor of the hydrogel matrix $\mathbf{F}_m$ may be expressed as follows:

$$\mathbf{F}_m = \frac{1}{1-2\rho}\left(\bar{\mathbf{F}} - 2\rho\mathbf{F}_p\right) \tag{8}$$

The deformation gradient tensor $\mathbf{F}_m$ may be multiplicatively split into a volumetric part $\mathbf{F}_{m\_\mathrm{vol}}$ and an isochoric part $\mathbf{F}_{m\_\mathrm{iso}}$ as:

$$\mathbf{F}_m = \mathbf{F}_{m\_\mathrm{vol}}.\mathbf{F}_{m\_\mathrm{iso}} \tag{9}$$

For an isotropic swelling, the two tensors are given by:

$$\mathbf{F}_{m\_\mathrm{vol}} = J_m^{1/3}\mathbf{I} \text{ and } \mathbf{F}_{m\_\mathrm{iso}} = J_m^{-1/3}\mathbf{F}_m \tag{10}$$

where $\mathbf{I}$ is the unit tensor.

The viscoelasticity in the material medium is based on the multiplicative decomposition concept of the deformation (Li et al., 2017). The deformation gradient tensor of the hydrogel matrix $\mathbf{F}_{m\_\mathrm{iso}}$ is then further multiplicatively split into an elastic part $\mathbf{F}^e_{m\_\mathrm{iso}}$ and a viscous part $\mathbf{F}^v_{m\_\mathrm{iso}}$ as :

$$\mathbf{F}_{m\_\mathrm{iso}} = \mathbf{F}^e_{m\_\mathrm{iso}}.\mathbf{F}^v_{m\_\mathrm{iso}} \tag{11}$$

The velocity gradient tensor of the hydrogel matrix $\mathbf{L}_{m\_\mathrm{iso}} = \dot{\mathbf{F}}_{m\_\mathrm{iso}}.\mathbf{F}^{-1}_{m\_\mathrm{iso}}$ is expressed as:

$$\mathbf{L}_{m\_\mathrm{iso}} = \mathbf{D}_{m\_\mathrm{iso}} + \mathbf{W}_{m\_\mathrm{iso}} \tag{12}$$

in which $\mathbf{D}_{m\_\mathrm{iso}}$ is the stretching rate tensor (symmetric part) and $\mathbf{W}_{m\_\mathrm{iso}}$ is the spin tensor (skew-symmetric part):

$$\mathbf{D}_{m\_\mathrm{iso}} = \frac{1}{2}\left(\mathbf{L}_{m\_\mathrm{iso}} + \mathbf{L}^T_{m\_\mathrm{iso}}\right) \text{ and } \mathbf{W}_{m\_\mathrm{iso}} = \frac{1}{2}\left(\mathbf{L}_{m\_\mathrm{iso}} - \mathbf{L}^T_{m\_\mathrm{iso}}\right) \tag{13}$$

Using the irrotationality hypothesis for the viscous flow (Gurtin and Anand, 2005), the viscous spin tensor is null $\mathbf{W}_{m\_\mathrm{iso}} = \mathbf{0}$ and the viscous deformation gradient tensor $\mathbf{F}^{v}_{m\_\mathrm{iso}}$ is governed by a differential equation of the general form:

$$\dot{\mathbf{F}}^{v}_{m\_\mathrm{iso}} = \mathbf{F}^{e^{-1}}_{m\_\mathrm{iso}}.\mathbf{D}^{v}_{m}.\mathbf{F}_{m\_\mathrm{iso}} \tag{14}$$

in which $\mathbf{D}^{v}_{m}$ is the viscous stretching rate tensor of the hydrogel matrix given by the following flow rule:

$$\mathbf{D}^{v}_{m} = \dot{\gamma}^{v}_{m}\frac{\boldsymbol{\sigma}_{m\_\mathrm{iso}}}{\left\|\boldsymbol{\sigma}_{m}\right\|} \tag{15}$$

where $\dot{\gamma}^{v}_{m}$ is the accumulated viscous strain rate, $\boldsymbol{\sigma}_{m\_\mathrm{iso}}$ is the isochoric part of the Cauchy stress tensor $\boldsymbol{\sigma}_{m}$ and $\left\|\boldsymbol{\sigma}_{m}\right\|$ is the effective stress expressed by the Frobenius norm:

$$\boldsymbol{\sigma}_{m\_\mathrm{iso}} = \boldsymbol{\sigma}_{m} - 1/3\,\mathrm{trace}\left(\boldsymbol{\sigma}_{m}\right)\mathbf{I} \text{ and } \left\|\boldsymbol{\sigma}_{m}\right\| = \sqrt{\mathrm{trace}\left(\boldsymbol{\sigma}_{m\_\mathrm{iso}}.\boldsymbol{\sigma}^{T}_{m\_\mathrm{iso}}\right)} \tag{16}$$

The accumulated viscous strain rate $\dot{\gamma}^{v}_{m}$ is expressed using a Bergstrom and Boyce (1998) formulation:

$$\dot{\gamma}^{v}_{m} = \frac{k_{v}}{\left(\sqrt{I^{v}_{1m}/3} - 1\right)^{\alpha}}\left\|\boldsymbol{\sigma}_{m}\right\| \tag{17}$$

where $I^{v}_{1m} = \mathrm{trace}\left(\boldsymbol{\varepsilon}^{v}_{m\_\mathrm{iso}}.\boldsymbol{\varepsilon}^{v^{T}}_{m\_\mathrm{iso}}\right)$ is the first invariant of the viscous part of the isochoric Hencky strain tensor $\boldsymbol{\varepsilon}_{m\_\mathrm{iso}} = \ln\mathbf{F}_{m\_\mathrm{iso}}$, k_{v} is the chains relaxation parameter and α is the stretch-dependency parameter.

The free energy of the hydrogel matrix ψ_{m} is additively split into a volumetric part ψ_{m_vol} and an isochoric part ψ_{m_iso} as:

$$\psi_{m} = \psi_{m\_\mathrm{vol}}\left(\varepsilon_{m\_\mathrm{vol}}\right) + \psi_{m\_\mathrm{iso}}\left(\mathbf{F}^{e}_{m\_\mathrm{iso}}\right) \tag{18}$$

The volumetric free energy of the hydrogel matrix ψ_{m_vol} is a function of the Hencky volumetric strain $\varepsilon_{m\_\mathrm{vol}} = \ln J_m$ (Holzapfel and Simo, 1996):

$$\psi_{m\_\mathrm{vol}} = \frac{1}{4} K_m \left(\exp\left(2\varepsilon_{m\_\mathrm{vol}}\right) - 1 - 2\varepsilon_{m\_\mathrm{vol}} \right) \tag{19}$$

The isochoric free energy of the hydrogel matrix ψ_{m_iso} is expressed as (Arruda and Boyce, 1993):

$$\psi_{m\_\mathrm{iso}} = \frac{n(t) k_\mathrm{B} T}{6} \int_{I^e_{1m0}}^{I^e_{1m}} \mathrm{L}^{-1}\left(\sqrt{\frac{I^e_{1m}}{3N(t)}} \right) \sqrt{\frac{3N(t)}{I^e_{1m}}}\, dI^e_{1m} \tag{20}$$

where $I^e_{1m} = \mathrm{trace}\left(\mathbf{C}^e_{m\_\mathrm{iso}}\right)$ is the first invariant of the elastic part of the isochoric Cauchy-Green deformation tensor $\mathbf{C}_{m\_\mathrm{iso}}$ of the matrix and $\mathrm{L}^{-1}(x)$ is the inverse Langevin function given by a Padé approximant $\mathrm{L}^{-1}(x) \approx x\left(3 - x^2\right)/\left(1 - x^2\right)$.

2.2.2. Nanoparticles

The description of the nanoparticles requires to take into consideration the local interaction between hydrogel matrix and inorganic reinforcement through the micromechanics framework. The Eshelbian homogenization provides an approximate solution for the problem of one particle embedded in an infinite domain. The Eshelby equivalent inclusion method consists to replace the particle domain by the matrix material by the introduction of an eigenstrain replacing the perturbed strain induced by the inhomogeneity. Following this method, Yin et al. (2002) obtained the averaged eigenstrain of a particle interacting with its neighboring nanoparticles by means of the Green function technique. Appendix A provides a summarize of the procedure.

The finite-strain kinematics of the particles are derived from Eq. (A12) of the equivalent homogeneous medium of the linear elastic two-phase media given in Appendix A. In virtue

of the Saint Venant-Kirchhoff assumption on hyperelastic media, the velocity gradient tensor of the particles $\mathbf{L}_p = \dot{\mathbf{F}}_p.\mathbf{F}_p^{-1}$ is expressed as:

$$\mathbf{L}_p = \mathbf{A}.\boldsymbol{\Gamma}.\left(\mathbf{I} - \phi\boldsymbol{\Gamma}\right)^{-1} : \bar{\mathbf{L}} \tag{21}$$

where $\bar{\mathbf{L}} = \dot{\bar{\mathbf{F}}}.\bar{\mathbf{F}}^{-1}$ is the macroscopic velocity gradient tensor of the nanocomposite, $\boldsymbol{\Gamma}$ is a tensor provided in Appendix A and $\mathbf{A}$ is the mismatch tensor:

$$\mathbf{A} = \left(\mathbf{K}_p - \mathbf{K}_m\right)^{-1}.\mathbf{K}_m \tag{22}$$

The free energy of the nanoparticles ψ_p is expressed through an ensemble-volume averaged homogenization procedure (Yin et al., 2002). It may be additively split into a volumetric part and an isochoric part as:

$$\psi_p = \left(\frac{\lambda_p}{2}\left(\chi_1 + 3\chi_2\right)^2 + \mu_p\left(2\chi_1\chi_2 + 3\chi_2^2\right)^2\right)\bar{\varepsilon}_{\text{vol}}^2 + \mu_p\chi_1^2\bar{\boldsymbol{\varepsilon}}_{\text{iso}} : \bar{\boldsymbol{\varepsilon}}_{\text{iso}} \tag{23}$$

where $\bar{\varepsilon}_{\text{vol}}$ is the Hencky volumetric strain, $\bar{\boldsymbol{\varepsilon}}_{\text{iso}} = \ln\bar{\mathbf{F}}_{\text{iso}}$ is the isochoric Hencky strain tensor, λ_p is the Lame's constant and, χ_1 and χ_1 are given by:

$$\chi_1 = \frac{1}{2w - M - \phi}\frac{\mu_m}{\mu_p - \mu_m} \text{ and } \chi_2 = \frac{1}{3\left(2w + 3m - M - \phi\right)}\frac{K_m}{K_p - K_m} - \frac{1}{3}\chi_1 \tag{24}$$

It is worth noticing that the local stress-strain response of the nanoparticles depends explicitly on the hydrogel matrix properties. Any perturbation of the local structure and dynamics of the hydrogel chains will affect the response of the nanoparticles as a result in changes of the near-field direct interactions.

2.3. Dynamic bonds

2.3.1. Stretching-retraction

Due to the large nanoparticle interfacial area, the nanoparticle surface contains a huge number of attaching groups which bond hydrogel chains having a chain length distribution

(Haraguchi et al., 2002) with a mean length N. The basic inelastic features in the material system during the course of a stretching followed by a retraction are illustrated in Fig. 1. The detachment mechanism is a progressive process, beginning with the shorter chains and progressing into the longer ones. At the initial stage, all links are intact. During the stretching stage, a number of chains may be detached from the nanoparticle surface leading to changes in chain length. The chains detachment mechanism acts first in the shorter chains (see the yellow, blue and red chains in the illustration) attached between nanoparticles pair whereas the longer chains (see the green chains in the illustration) continue to sustain the chains network integrity. A hysteresis loop is then formed due to the concomitant contribution upon retraction of the chain re-attachment mechanism and the viscous effects. The re-attachment mechanism may be done in new positions (see the yellow chains in the illustration). The mean length of the elastically active chains $N(t)$ should be always larger than its reference $N_0 = N(t=0)$ whereas the mean chain density of the elastically active chains $n(t)$ should be always smaller than its reference $n_0 = n(t=0)$. We express these two physical quantities as follows:

$$N(t) = \frac{N_0}{N_{on/off}} \text{ and } n(t) = n_0 N_{on/off} \tag{25}$$

where the term $N_{on/off}$ is defined by the following kinetics:

$$\dot{N}_{on/off} = 1 - N_{on/off}\left(1 + k_{on/off}\right) \tag{26}$$

in which $k_{on/off}$ is the rate of attachable and detachable bonds given by:

$$k_{on/off} = k_{on/off\_0} \exp\left(\frac{\|\boldsymbol{\sigma}_m\|}{\sigma_{off} N_{on/off}}\right) \tag{27}$$

where k_{on/off_0} is a material constant and σ_{off} is a scale factor controlling the bonds strength.

A key point of our theory, the quantity $N_{on/off}$ is a decreasing function of the applied strain upon stretching and an increasing function of the applied strain upon retraction. The stress in the hydrogel matrix drives these opposite evolutions of $N_{on/off}$ by the rate of attachable and detachable bonds $k_{on/off}$. The evolutions affect in turn the interfacial characteristics and thus the bond strength between the two phases. At the end of the stretching-retraction process applied to the nanocomposite, the network recovers its initial features such that:

$$N(t)=N_0 \text{ and } n(t)=n_0 \tag{28}$$

Nonetheless, the equilibrium state is not reached at the end of the mechanical loading since a strain amount remains retained in the hydrogel system at the loading time-scale.

To disclose some important indications concerning the chains behavior in interaction with the particles features, Fig. 3 presents an illustrative example of the chain force evolution with the applied strain for different particle radii while the particle amount is kept constant. The model parameters are those used for Fig. 4b. The model shows that the chain stiffness decreases distinctly with the decrease in particle radius and particle amount. Whereas in the case of a purely elastic response the chain force will become infinite at the limiting extension, the detachment mechanism leads to the progressive stiffness reduction and the appearance of a peak in the chain force evolution. When the particle amount increases, the chain damage occurs earlier and the critical strain involved in the peak force is distinctly decreased.

2.3.2. Self-healing

When the nanocomposite is unloaded down to a free stress, i.e. $\bar{\boldsymbol{\sigma}}=\mathbf{0}$, an amount of the strain is instantaneously recovered whereas another amount necessitates a longer recovery time (see the illustration in Fig. 1). The different parts of the deformation gradient tensors $\bar{\mathbf{F}}\neq\mathbf{I}$, $\mathbf{F}^{v}_{m\_\mathrm{iso}}\neq\mathbf{I}$, $\mathbf{F}^{e}_{m\_\mathrm{iso}}\neq\mathbf{I}$ and $\mathbf{F}_{p}\neq\mathbf{I}$ are related by using Eq. (8):

$$\mathbf{F}^{v}_{m\_\mathrm{iso}}\mathbf{F}^{e}_{m\_\mathrm{iso}}=\frac{1}{1-2\rho}\left(\bar{\mathbf{F}}-2\rho\mathbf{F}_{p}\right) \tag{29}$$

Considering volume preserving, Eq. (3) is re-written as:

$$\left(1-2\rho\right)\boldsymbol{\sigma}_{m\_\mathrm{iso}}+\phi\boldsymbol{\sigma}_{p\_\mathrm{iso}}=\mathbf{0} \tag{30}$$

where the Cauchy stress tensors $\boldsymbol{\sigma}_{m\_\mathrm{iso}}$ and $\boldsymbol{\sigma}_{p\_\mathrm{iso}}$ may be expressed as:

$$\left[\boldsymbol{\sigma}_{m\_\mathrm{iso}}\right]_{i}=\frac{\lambda^{e}_{m\_i}}{J_{m}}\frac{\partial\psi_{m\_\mathrm{iso}}}{\partial\lambda^{e}_{m\_i}}=\frac{\lambda^{e}_{m\_i}}{J_{m}}\frac{\partial\psi_{m\_\mathrm{iso}}}{\partial I^{e}_{1m}}\frac{\partial I^{e}_{1m}}{\partial\lambda^{e}_{m\_i}}\ \text{and}\ \left[\boldsymbol{\sigma}_{p\_\mathrm{iso}}\right]_{i}=\frac{\lambda_{p\_i}}{J_{p}}\frac{\partial\psi_{p\_\mathrm{iso}}}{\partial\lambda_{p\_i}} \tag{31}$$

No summation on *i* is implied in this equation.

From Eqs. (14), (15), (17) and (30), the viscous deformation gradient tensor $\mathbf{F}^{v}_{m\_\mathrm{iso}}$ can be extracted:

$$\dot{\mathbf{F}}^{v}_{m\_\mathrm{iso}}=-\frac{k_{v}}{\left(\sqrt{I^{v}_{1m}/3}-1\right)^{\alpha}}\frac{\phi}{1-2\rho}\mathbf{F}^{v}_{m\_\mathrm{iso}}.\boldsymbol{\sigma}_{p\_\mathrm{iso}} \tag{32}$$

Using Eq. (29) and (30), $\mathbf{F}^{e}_{m\_\mathrm{iso}}$ and $\bar{\mathbf{F}}$ are calculated upon a creep condition at zero-stress. The parameter k_{v} controls the hydrogel chains relaxation during the different loading stages. To consider the stretching-retraction asymmetry of the gel rate-sensitivity, the following expression is retained (Lin et al., 2020):

$$k_{v}=k_{v\_0}\left(1+\left|\frac{\dot{\lambda}}{\dot{\lambda}_{0}}\right|\right)^{\tau}\exp\left(\mathrm{sgn}\left(\dot{\lambda}\right)\right) \tag{33}$$

in which k_{v_0} is the viscous multiplier, τ is the rate-dependency factor and $\dot{\lambda}_{0}$ is the reference loading rate. The term $\mathrm{sgn}\left(\dot{\lambda}\right)$ signifies:

$$\mathrm{sgn}\left(\dot{\lambda}\right)=\begin{cases}+1 & \text{for stretching} \quad \left(\dot{\lambda}>0\right)\\ -1 & \text{for retraction} \quad \left(\dot{\lambda}<0\right)\\ 0 & \text{for recovery} \quad \left(\dot{\lambda}=0\right)\end{cases} \tag{34}$$

By constitutively relating the nanostructure and the overall nanocomposite behavior, the model may be employed to better understand the mechanisms of mechanical property enhancement. To this goal, the following important features will be examined by comparisons with available experimental data of a variety of nanocomposite systems:

- The stretching-retraction cycle of nanocomposite system in connection to the chains detachment-attachment mechanism and the nanoparticle-matrix interaction as illustrated in Fig. 1.
- The complete failure of nanocomposite system when the network losses all connectivity.
- The self-healing response of nanocomposite system when the network recovers its equilibrium state.

3. Comparison with experiments

The model contains very few inputs listed in Table 1 for which the physical meaning is provided. Some of them (elastic constants of phases, chains network features and amount of phases) have direct physical meaning while others (related to viscosity and bonds dissociation/re-association) are physically interpretable.

In what follows, the effects of various microstructures on the macro-response are considered by examining nanofiller type, nanofiller concentration and hydrogel chains network features. The examined macro-behaviors include monotonic stress-strain response till failure and some inelastic features such as rate-dependency, hysteresis, continuous relaxation and room temperature self-healing facility. Some data are used to fit the model parameters while others are used to verify the model predictability. All stress and strain quantities are defined in their nominal form.

3.1. Stretchability and strength

In this section, the model calibrations are compared to monotonic stress-strain experimental data taken from the work of Liu et al. (2019). The hydrogel systems are made of metal-organic framework (MOF) (ZIF-8, ZIF-67, UiO-66) and SiO_2. The hydrogel systems are designated as X-Y-Z (X being the filler type, Y the filler amount and Z the cross-linker amount). The tests have been performed at room temperature under a constant stretch rate of 30 min^{-1}. Figs. 4 and 5 present the comparison between micromechanical model simulations and experimental data in which several microstructure factors having a significant impact are examined. Model simulations are presented as lines while experimental data are presented as symbols. The computed stress is presented till failure that is defined as the local maximum stress. Unless explicitly otherwise stated, the model inputs are those listed in Table 1. They correspond to a cross-linker amount of 1 mg and a filler amount of 10%. They were obtained through a fitting optimization based on the minimization of differences between model simulations and experimental data. Figs. 6 and 7 completes the identification results with the parameters affected by the cross-linker and filler amounts. The values must be seen as average values incorporating variability effects and the trends will be used to bring a better understanding of reinforcement mechanisms.

3.1.1. Pure hydrogel

Prior to compare with the data of nanocomposites, Fig. 4a presents the comparison between model simulations and stress-strain experimental data of the pure hydrogel (designated as matrix-1 in Table 1) including different cross-linker amounts (1, 5, 10 and 40 mg). The obvious increase in stiffness and decrease in stretchability with the increase in cross-linker amount is the direct consequence of chemical microstructure change, that is, an increase in mean density and strength of elastically active chains (along with a decrease in mean length

of elastically active chains) as shown in Fig. 6a. Bonds strength in pure hydrogel is slightly modified with the variation in cross-linker amount but chains viscosity remains constant as evidenced in Fig. 7a.

3.1.2. Filler amount

Fig. 4b presents the stress-strain curves of the hydrogel-ZIF-8 systems for different filler amounts using hydrogel as the matrix. The presence of nanoparticles is likely to modify the molecular organization and dynamics of the hydrogel chains as compared to the pure hydrogel. The dispersion of 10% nanoparticles in the hydrogel leads to a remarkable increase of ductility. When the amount of nanoparticles increases from 10% to 20%, the contact area between nanoparticles and hydrogel matrix is extremely magnified. As a consequence, the stretchability decreases but the mechanical strength significantly increases, indicating that adding more ZIF-8 nanofillers leads to a loss of mobility of hydrogel chains in the vicinity of nanofillers that strengthens the whole hydrogel network (Figs. 6b and 7b). Due to the increased level of interactions between the hydrogel chains and the nanoparticles, the chains viscosity is also increased.

3.1.3. Filler type

The application of our model is extended to the other types of reinforcing elements (namely ZIF-67, UiO-66 and SiO_2) in Fig. 5. While the model is capable of fitting the experimental data reasonably well, it can bring some physical interpretations in particular on the complex interaction between nanofillers and hydrogel matrix. The level of overall property enhancement is controlled by the strong nanoparticle-matrix interactions and the mobility changes at the nano-scale. Inevitably, the higher level of interaction, the larger the perturbed region of polymer matrix surrounding the nanoparticle (Boutaleb et al., 2009). Table 1 shows

a modification of the properties of the hydrogel inside the nanocomposite, as compared to those of the neat hydrogel. The nanoparticles act as additional crosslinking points to strengthen the network but the strength of interactions varies from a nanofiller type to another which impacts differently the stretchability and the mechanical strength of the nanocomposite. The evolution of the chains network due to progressive chains detachment mechanism is presented in Fig. 8a till its complete loss of load-bearing capability. Also, the interfacial interaction between hydrogel matrix and nanoparticles is affected by the hydrogel response evolution that in turn affects the nanoparticles response. As shown in Fig. 8b, the stress magnitude in the nanoparticles depends on their nature and the gradual weakening of bonds between the two phases. This local response can be connected to the macroscopic mechanical properties given in Fig. 5a in particular to the maximum strain and stress levels reached by the nanocomposite before final failure. The ZIF-8-10%-M1 and ZIF-67-10%-M1 hydrogels exhibit quite similar stretchability whereas the UiO-66-10%-M1 hydrogel is slightly less stretchable than the ZIF systems but with a significantly higher mechanical strength. The SiO_2-10%-M1 hydrogel has the lowest ductility but the highest toughening effects with a great mechanical strength improvement. The reinforcement mechanisms are generally ascribed to electrostatic interactions between the hydrogel chains and the nanofillers. Stronger near-field direct interactions result in better mechanical properties of the hydrogel-based nanocomposites. In MOF nanofillers (ZIF and UiO), the polar groups and cationic metal centers on the nanoparticle surface act as anchoring points for hydrogel chains (Liu et al., 2019). The latter results in an increase in mean chain density (see Table 1 and Fig. 6). The insolubility and aggregation of SiO_2 nanofillers leads to higher crosslinking points in hydrogel, compared to MOF nanofillers, and to a higher mean chain density. The ZIF-8 and SiO_2 nanofillers reinforcement is also examined in Fig. 5b for different cross-linker amounts. The increase in cross-linker amount profoundly modifies the chains network properties as

reported in Figs. 6a and 7a. Both mean length and density evolve with cross-linker amount but in an opposite manner. The toughening effects of the hydrogels are also largely determined by the strength of nanofillers-matrix interactions and the competition between elasticity and strength of the temporarily attached chains. Note that the effects of the cross-linker amount on the macro-stress are directly connected to the local properties evolution in the hydrogel and depends on the nanofiller type. The monotonic macro-stress evolution of the SiO_2 hydrogel with cross-linker amount implies a monotonic evolution of the network properties as observed in the plots of Figs. 6a and 7a. The network monotonic evolution is not expected for the ZIF-8 hydrogel since its macro-stress at failure increases with the cross-linker amount to reach a maximum value and falls beyond this value. Fig. 6a shows that the bonds strength in the ZIF-8 hydrogel follows the same trends. Also, the nanofiller-matrix interaction leads to an alteration of the network properties, amplified by the filler amount as observed in the plots of Figs. 6b and 7b.

3.2. Inelastic features

In this section, the model is applied to some history-dependent features (such as rate-dependent stress-strain till failure, hysteresis and continuous relaxation) of hydrogel-based nanocomposites with metal-coordinated Fe^{3+} bonds taken from the work of Lin et al. (2020).

3.2.1. Rate-dependent stretchability and strength

Fig. 9 shows that our model is able to provide a good representation of the monotonic stress-strain response for the different stretching rates. Again, the micromechanical model results are presented till failure that is defined as the local maximum stress. The inputs required by the modeling are listed in Table 1 in which the bonds strength parameter σ_{off} and the viscous multiplier k_{v_0} are expressed as follows:

$$\sigma_{off} = -3.73\exp\left(-2.9\times10^{-1}\dot{\lambda}\right) + 6.40 \tag{35}$$

$$k_{v\_0} = -2.34\exp\left(-4.2\times10^{-2}\dot{\lambda}\right) - 2.48 \tag{36}$$

While these data provide a good first verification of the model, Figs. 10-14 present some model predictions for various key loading conditions governing the hydrogel mechanics. The goal is to further verify the predictive capacities of the model and to better understand the relation between macro-response and mechanisms of nanofillers reinforcement.

3.2.2. Stress hysteresis

Fig. 10 shows how the model can reproduce the hydrogel mechanics during stretching-retraction cycles at different maximum stretch levels and stretch rates, respectively. In these simulations, the macroscopic stretch is ramped to a pre-determined level at a constant rate and then ramped down to zero-stress at the same absolute constant rate. The pronounced hysteresis loops displayed by the material upon the cyclic loading is well captured by the model along with the increase in loop area (along with the related dissipated energy) with increasing applied strain. During the hydrogel retraction stage, the unloading path shape is not well replicated by the model what a fine analysis of the model results has attributed to the particles response. The effect of the applied strain on the recovery extent at the end of the retraction segment is nonetheless well captured by the model. It is therefore able to connect the nanostructure, the dissociation and re-association mechanism of the shorter hydrogel chains and the macroscopic stress hysteresis of the nanocomposite system (see Fig. 1).

3.2.3. Stress relaxation

We examine also the model capabilities under continuous relaxation. In these simulations, the macroscopic stretch is ramped to a pre-determined level at a constant rate and then kept constant for a prescribed delay. As depicted in Fig. 11, the model is able to reproduce the

different features of the Fe^{3+} hydrogel mechanics upon continuous relaxation at different maximum stretch levels and stretch rates, respectively. These adequate agreements further confirm the validity of our approach.

3.2.4. Self-healing

To illustrate further the model capabilities, the capacity of the hydrogels to restore, by self-healing, initial microstructure and mechanical strength, in relation to loading conditions and microstructure features, is now treated. Fig. 12 shows the capability of our model to evaluate the room temperature self-healing of the Fe^{3+} hydrogel for different recovery times. In the simulations, a creep at zero-stress is carried out for a prescribed waiting delay between each stretching-retraction cycle. The second cycle is reported in the figure in order to replicate the same conditions than the experiments of Lin et al. (2020), an amount of remanent strain (at zero-stress) still remaining after the partial strain recovery. The creep process, corresponding to the course of the recovery from non-equilibrium state (at the retraction instant) to equilibrium state when the hydrogel recovers its initial conformation, is driven in our theory by the formulae of Section 2.3.2. In agreement with the experimental observations, the model simulations show that the mechanical strength and the hysteresis loop become progressively larger with the waiting time, indicating the gradual recovery of the hydrogel-based nanocomposite. It is satisfactory to point out that the waiting time of eight hours for the nearly full recovery is well captured by the model. The proper description of the stress-strain curves till failure as well the hysteresis, the continuous relaxation and the room temperature self-healing facility demonstrates that the microstructure monitoring via the model seems physically realistic.

It should be emphasized that one of the most important capability of the proposed model is related to self-healing predictions that may be related to loading histories and microstructure

features. The strain evolution during recovery at zero-stress of the hydrogel-based $Fe3^{+}$ nanocomposites is plotted in Fig. 13 as a function of recovery time such that a curved profile is obtained by considering the following expression for the strain recovery R:

$$R = \left(1 - \frac{\varepsilon}{\varepsilon_{\max}}\right) \times 100 \tag{37}$$

where ε and $\varepsilon_{\max}$ are, respectively, the nominal strain stored in the hydrogel and its maximum value. The strain recovery starts to increase linearly with the recovery time and rapidly exhibits a curved profile which tends towards a stabilized state for which there is no strain recovery change. The reached maximum recovery extent corresponds to the equilibrium state. Similar profiles are obtained in other traditional polymeric systems (Su and Peng, 2018; Shen et al., 2019; Cherief et al., 2020; Dai et al., 2020) but with a strain recovery requiring a quasi-infinite duration at room temperature. Fig. 13 depicts the effect of loading conditions (stretch levels and stretch rates) on the self-healing response. It can be observed that the higher the strain level, the higher the recovery extent. Due to higher hydrogel chains relaxation at the lowest stretch rate, the time-dependent recovery becomes significantly higher with less elastic energy.

Numerical simulations are carried out to address the influence of microstructure features on the self-healing facility of hydrogel systems examined in Section 3.1. Fig. 14 provides important indications concerning the complex nanofiller-matrix interaction on the self-healing facility due to variations in nanofiller type and cross-linker amount. Fig. 14a shows that the recovery extent varies from a nanofiller type to another which indicates the great complexity of the history-dependent features of hydrogel systems. This prediction is possible because the reinforcing effect of nanoparticles is introduced in the model. The micromechanical model results in Fig. 14b show that the cross-linker amount is also another key microstructure parameter governing the response. It can be observed that the increase in

cross-linker amount enhances the self-healing ability. The micromechanical model simulations demonstrate that for the evaluation of the self-healing response, it is fundamental to consider the simultaneous effects of the different internal network features related to the nanoparticles and the hydrogel matrix. This prediction can only be made if they are explicit inputs of the modeling approach.

3.3. Biaxial loading effect

As a final point of discussion, the model capabilities to describe the biaxial behavior of hydrogel systems is presented. The model is expected to predict the visco-super-elastic response under any biaxial loading path. Nonetheless, multiaxial experiments on hydrogel systems are rarely documented in the literature. As far as we know, only the work of Mai et al. (2018) exists to date and only for a pure hydrogel stretched under equibiaxial (EB), unequal biaxial (UB) with a 0.5 biaxiality ratio and planar (P) loadings. Fig. 15 provides a schematic representation of these biaxial loading paths. All experiments have been performed at room temperature under a constant stretch rate of 1.2 min^{-1}. Fig. 15 provides the experimental data of Mai et al. (2018) and the computed stress as a function of the applied strain along the maximum principal direction. The model parameters were identified from the EB response of the pure hydrogel (designated as matrix-2 in Table 1) and the same model parameters were then used to predict the UB and P curves. It is satisfactory to observe that the model provides an acceptable description of the nonlinear stress response and the peak (failure) stress.

The predicted stretches at failure are plotted in Fig. 16 under a wider range of biaxiality ratios such that a failure envelope is obtained with a symmetry relative to the main bisectrix. The model is also used in Fig. 16 to predict the effect of nanofillers reinforcement on the biaxial failure envelope. The insertion of inorganic nanoparticles into the matrix-2 is performed

using the same amplifying effect obtained for the matrix-1 properties for the nanofiller types examined in Section 3.1. The larger failure envelope is obtained for the ZIF-8 hydrogel and the smaller one for the the SiO_2 hydrogel.

4. Concluding remarks

The aim of this paper was to propose a quantitative prediction of the mechanics of visco-super-elastic hydrogel-based nanocomposites. Using the concept of cubic material volume combined with the Eshelby equivalent inclusion method, the continuum-based model connects the macro-response to internal network physics starting from the nanostructure. The model is used to relate the reinforcing effect of nanoparticles to overall properties such as stretchability, mechanical strength, stress hysteresis and self-healing response. Quantitative comparisons with available experiments show the relevance of the model for a variety of hydrogel-nanofiller material systems. The model contains very few physically interpretable material constants and appears as a valuable tool for the reliable design of such new material systems.

Appendix A

From the Eshelby equivalent inclusion method under infinitesimal elastic theory, the local strain fields $\boldsymbol{\varepsilon}$ may be expressed at any local point $\boldsymbol{r}$ of the domain occupied by the nanoparticles Ω_p and by the hydrogel matrix Ω_m (Ju and Sun, 1999):

$$\boldsymbol{\varepsilon}(\boldsymbol{r}) = \mathbf{K}_m^{-1} : \boldsymbol{\sigma}(\boldsymbol{r}) + \boldsymbol{\varepsilon}^*(\boldsymbol{r}) \text{ for } \boldsymbol{r} \in \Omega_p \text{ and } \boldsymbol{\varepsilon}(\boldsymbol{r}) = \mathbf{K}_m^{-1} : \boldsymbol{\sigma}(\boldsymbol{r}) \text{ for } \boldsymbol{r} \in \Omega_m \qquad \text{(A1)}$$

where $\boldsymbol{\sigma}(\boldsymbol{r})$ is the local stress and $\boldsymbol{\varepsilon}^*$ is the equivalent eigenstrain.

The interaction of the central nanoparticle with its eight neighboring nanoparticles is considered by means of the Green function technique. At any local point $\boldsymbol{r}$ of the central

nanoparticle P_0, the perturbed strain $\boldsymbol{\varepsilon}'(\boldsymbol{r})$ can be related to the eigenstrain $\boldsymbol{\varepsilon}^*(\boldsymbol{r})$ as the sum of the perturbation contribution from the central nanoparticle itself and the effect from the local points $\boldsymbol{r}'$ in the eight neighboring nanoparticles:

$$\boldsymbol{\varepsilon}'(\boldsymbol{r}) = \mathbf{S} : \boldsymbol{\varepsilon}^*(\boldsymbol{r}) + \sum_{i=1}^{n=8} \int_{\Omega_i} \mathbf{G}(\boldsymbol{r} - \boldsymbol{r}') : \boldsymbol{\varepsilon}^*(\boldsymbol{r}') \mathrm{d}\boldsymbol{r}' \tag{A2}$$

where $\mathbf{S}$ is the Eshelby tensor and $\mathbf{G}$ is the fourth-rank Green function:

$$G_{ijkl}(\boldsymbol{r} - \boldsymbol{r}') = \frac{1}{8\pi(1-\nu_m)\bar{r}^3} \begin{bmatrix} (1-2\nu_m)(\delta_{ik}\delta_{jl} + \delta_{il}\delta_{jk} - \delta_{ij}\delta_{kl}) \\ +3\nu_m(\delta_{ik}n_j n_l + \delta_{il}n_j n_k + \delta_{jk}n_i n_l + \delta_{jl}n_i n_k) \\ +3\delta_{ij}n_k n_l + 3(1-2\nu_m)\delta_{kl}n_i n_j - 15 n_i n_j n_k n_l \end{bmatrix} \tag{A3}$$

in which δ_{ij} is the Kronecker delta, $\bar{r} = \|\boldsymbol{r} - \boldsymbol{r}'\|$, $\boldsymbol{n} = (\boldsymbol{r} - \boldsymbol{r}')/\bar{r}$ and ν_m is the Poisson's ratio of the hydrogel matrix.

The volume averaged eigenstrain $\bar{\boldsymbol{\varepsilon}}^*_{\Omega_0}$ over the domain occupied by the central nanoparticle is:

$$-\mathbf{A} : \bar{\boldsymbol{\varepsilon}}^*_{\Omega_0} = \boldsymbol{\varepsilon}_0 + \mathbf{S} : \bar{\boldsymbol{\varepsilon}}^*_{\Omega_0} + \mathbf{g} : \bar{\boldsymbol{\varepsilon}}^*_{\Omega_0} \tag{A4}$$

where $\boldsymbol{\varepsilon}_0$ is the far-field strain ($\boldsymbol{\varepsilon}_0 = \mathbf{K}_m^{-1} : \boldsymbol{\sigma}_0$ with $\boldsymbol{\sigma}_0$ the far-field stress) and $\boldsymbol{g}$ is the interaction term:

$$\boldsymbol{g} = \frac{1}{\Omega_m} \sum_{i=1}^{n=8} \int_{\Omega_m} \int_{\Omega_i} \mathbf{G}(\boldsymbol{r} - \boldsymbol{r}') \mathrm{d}\boldsymbol{r}\, \mathrm{d}\boldsymbol{r}' \tag{A5}$$

Yin et al. (2002) derived the following relationship of the volume averaged eigenstrain $\bar{\boldsymbol{\varepsilon}}^*_{\Omega_0}$:

$$\bar{\boldsymbol{\varepsilon}}^*_{\Omega_0} = -\boldsymbol{\Gamma} : \boldsymbol{\varepsilon}_0 \tag{A6}$$

where $\boldsymbol{\Gamma}$ is a tensor given by:

$$\Gamma_{ijkl} = \left(\frac{-m}{(2w - M)(2w + 3m - M)} + \frac{M}{2w(2w - M)} \delta_{IK} \right) \delta_{ij}\delta_{kl} + \frac{1}{4w}(\delta_{ik}\delta_{jl} + \delta_{il}\delta_{jk}) \tag{A7}$$

in which m, w and M are given by:

$$m=\frac{1}{3}\left(\frac{K_m}{K_p-K_m}-\frac{\mu_m}{\mu_p-\mu_m}\right)+\frac{5\nu_m-1}{15(1-\nu_m)}+\frac{M}{5} \tag{A8}$$

$$w=\frac{1}{2}\frac{\mu_m}{\mu_p-\mu_m}+\frac{4-5\nu_m}{15(1-\nu_m)}+\frac{M}{5} \tag{A9}$$

$$M=\frac{40\left(14\rho^2-5\right)\rho^3}{45(1-\nu_m)} \tag{A10}$$

The governing constitutive equations of the equivalent homogeneous medium of the linear elastic two-phase medium are given by the following relationships (Yin et al., 2002):

$$\bar{\boldsymbol{\sigma}}=\bar{\mathbf{K}}:\bar{\boldsymbol{\varepsilon}}^e=\mathbf{K}_m:\boldsymbol{\varepsilon}_0 \tag{A11}$$

$$\bar{\boldsymbol{\varepsilon}}^e=\left(\mathbf{I}-\phi\boldsymbol{\Gamma}\right).\boldsymbol{\Gamma}^{-1}.\mathbf{A}^{-1}:\boldsymbol{\varepsilon}_p \tag{A12}$$

$$\boldsymbol{\varepsilon}_0=\left(\mathbf{I}-\phi\boldsymbol{\Gamma}\right)^{-1}:\bar{\boldsymbol{\varepsilon}}^e \tag{A13}$$

where $\bar{\boldsymbol{\sigma}}$ and $\bar{\boldsymbol{\varepsilon}}^e$ are the ensemble-volume averaged (macroscopic) stress and elastic strain tensors and $\bar{\mathbf{K}}$ is the macroscopic stiffness tensor.

Acknowledgments

This work was financially supported by the Algerian National Exceptional Program, the General Directorate for Scientific Research and Technological Development in Algeria and the Algerian Ministry of Higher Education and Scientific Research.

References

Arruda, E.M., Boyce, M.C., 1993. A three-dimensional constitutive model for the large stretch behavior of rubber elastic materials. Journal of the Mechanics and Physics of Solids 41, 389-412.

Bergstrom, J.S, Boyce, M.C., 1998. Constitutive modeling of the large strain time-dependent behavior of elastomers. Journal of the Mechanics and Physics of Solids 46, 931-954.

Bhattacharya, S., Samanta, S.K., 2016. Soft-nanocomposites of nanoparticles and nanocarbons with supramolecular and polymer gels and their applications. Chemical Reviews 116, 11967-12028.

Boutaleb, S., Zaïri, F., Mesbah, A., Naït-Abdelaziz, M., Gloaguen, J.M., Boukharouba, T., Lefebvre, J.M., 2009. Micromechanics-based modelling of stiffness and yield stress for

silica/polymer nanocomposites. International Journal of Solids and Structures 46, 1716-1726.
Chen, H., Liu, Y., Ren, B., Zhang, Y., Ma, J., Xu, L., Chen, Q., Zheng, J., 2017. Super bulk and interfacial toughness of physically crosslinked double-network hydrogels. Advanced Functional Materials 27, 1703086.
Cherief, M.N.D., Zaïri, F., Ding, N., Gloaguen, J.M., Naït-Abdelaziz, M., Benguediab, M., 2020. Plasticity and thermally-induced recovery in polycarbonate. Mechanics of Materials 148, 103515.
Dai, L., Tian, C., Xiao, R., 2020. Modeling the thermo-mechanical behavior and constrained recovery performance of cold-programmed amorphous shape-memory polymers. International Journal of Plasticity 127, 102654.
Dargazany, R., Khiem, V.N., Itskov, M., 2014. A generalized network decomposition model for the quasi-static inelastic behavior of filled elastomers. International Journal of Plasticity 63, 94-109.
Deng, Z., Hu, T., Lei, Q., He, J., Ma, P.X., Guo, B., 2019. Stimuli-responsive conductive nanocomposite hydrogels with high stretchability, self-healing, adhesiveness, and 3D printability for human motion sensing. ACS Applied Materials and Interfaces 11, 6796–6808.
Drozdov, A.D., Christiansen, J.D., 2018. Nanocomposite gels with permanent and transient junctions under cyclic loading. Macromolecules 51, 1462-1473.
Drozdov, A.D., Christiansen, J. de C., 2020. Tension-compression asymmetry in the mechanical response of hydrogels. Journal of the Mechanical Behavior of Biomedical Materials 110, 103851.
Farahani, R.D., Dubé, M., Therriault, D., 2016. Three-dimensional printing of multifunctional nanocomposites: Manufacturing techniques and applications. Advanced Materials 28, 5794-821.
Guo, Q., Zaïri, F., 2021. A micromechanics-based model for deformation-induced damage and failure in elastomeric media. International Journal of Plasticity 140, 102976.
Guo, Q., Zaïri, F., 2020. A physically-based thermo-mechanical model for stretch-induced crystallizable rubbers: Crystallization thermodynamics and chain-network crystallization anisotropy. International Journal of Plasticity 131, 102724.
Guo, Y., Bae, J., Zhao, F., Yu, G., 2019. Functional hydrogels for next-generation batteries and supercapacitors. Trends in Chemistry 1, 335-348.
Guo, Q., Zaïri, F., Guo, X., 2018. A thermo-viscoelastic-damage constitutive model for cyclically loaded rubbers. Part I: Model formulation and numerical examples. International Journal of Plasticity 101, 106-124.
Guo, J., Long, R., Mayumi, K., Hui, C.Y., 2016. Mechanics of a dual cross-link gel with dynamic bonds: Steady state kinetics and large deformation effects. Macromolecules 49, 3497-3507.
Gurtin, M.E., Anand, L., 2005. The decomposition $F=F^eF^p$, material symmetry, and plastic irrotationality for solids that are isotropic-viscoplastic or amorphous. International Journal of Plasticity 21, 1686-1719.
Haraguchi, K., Takehisa, T., Fan, S., 2002. Effects of clay content on the properties of nanocomposite hydrogels composed of poly (N-isopropylacrylamide) and clay. Macromolecules 35, 10162-10171.
Holzapfel, G., Simo, J., 1996. Entropy elasticity of isotropic rubber-like solids at finite strains. Computer Methods in Applied Mechanics and Engineering 132, 17-44.
Ju, J.W., Sun, L.Z., 1999. A novel formulation for exterior point Eshelby's tensor of an ellipsoidal inclusion. Journal of Applied Mechanics 66, 570-574.

Kulcu, I.D., 2019. Characterization of stress softening and self-healing in a double network hydrogel. Results in Physics 12, 1826-1833.
Kumar, G.G., Hashmi, S., Karthikeyan, C., GhavamiNejad, A., Vatankhah-Varnoosfaderani, M., Stadler, F.J., 2014. Graphene oxide/carbon nanotube composite hydrogels-versatile materials for microbial fuel cell applications. Macromolecular Rapid Communications 35, 1861-1865.
Li, Y., He, Y., Liu, Z., 2017. A viscoelastic constitutive model for shape memory polymers based on multiplicative decompositions of the deformation gradient. International Journal of Plasticity 91, 300-317.
Li, Y., Tang, S., Kroger, M., Liu, W.K., 2016. Molecular simulation guided constitutive modeling on finite strain viscoelasticity of elastomers. Journal of the Mechanics and Physics of Solids 88, 204-226
Lima-Tenorio, M.K., Tenorio-Neto, E.T., Guilherme, M.R., Garcia, F.P., Nakamura, C.V., Pineda, E.A.G., Rubira, A.F., 2015. Water transport properties through starch-based hydrogel nanocomposites responding to both pH and a remote magnetic field. Chemical Engineering Journal 259, 620-629.
Lin, J., Zheng, S.Y., Xiao, R., Yin, J., Wu, Z.L., Zheng, Q., Qian, J., 2020. Constitutive behaviors of tough physical hydrogels with dynamic metal-coordinated bonds. Journal of the Mechanics and Physics of Solids 139, 103935.
Liu, Y., Zhang, H., Zheng, Y., 2016. A micromechanically based constitutive model for the inelastic and swelling behaviors in double network hydrogels. Journal of Applied Mechanics 83, 021008.
Liu, H., Peng, H., Xin, Y., Zhang, J., 2019. Metal-organic frameworks: A universal strategy towards super-elastic hydrogels. Polymer Chemistry 10, 2263-2272.
Long, R., K. Mayumi, C., Creton, T., Narita, Hui C.Y., 2014. Time dependent behavior of a dual cross-link self-healing gel: Theory and experiments. Macromolecules, 47, 7243-7250.
Lu, T., Wang, Z., Tang, J., Zhang, W., Wang, T., 2020. A pseudo-elasticity theory to model the strain-softening behavior of tough hydrogels. Journal of the Mechanics and Physics of Solids 2020, 103832.
Mahjoubi, H., Zaïri, F., Tourki, Z., 2019. A micro-macro constitutive model for strain-induced molecular ordering in biopolymers: application to polylactide over a wide range of temperatures. International Journal of Plasticity 123, 38-55.
Mai, T.T., Matsuda, T., Nakajima, T., Gong, J.P., Urayama, K., 2018. Distinctive characteristics of internal fracture in tough double network hydrogels revealed by various modes of stretching. Macromolecules 51, 5245-5257.
Mao, Y., Lin, S., Zhao, X., Anand, L., 2017. A large deformation viscoelastic model for double-network hydrogels. Journal of the Mechanics and Physics of Solids 100, 103-130.
Merino, S., Martin, C., Kostarelos, K., Prato, M., Vazquez, E., 2015. Nanocomposite hydrogels: 3D polymer-nanoparticle synergies for on-demand drug delivery. ACS Nano 9, 4686-4697.
Morovati, V., Dargazany, R., 2019. Micro-mechanical modeling of the stress softening in double-network hydrogels. International Journal of Solids and Structures 164, 1-11.
Sarvestani, A.S., He, X., Jabbari, E., 2008. The role of filler-matrix interaction on viscoelastic response of biomimetic nanocomposite hydrogels. Journal of Nanomaterials 2008, 1-9.
Schexnailder, P., Schmidt, G., 2009. Nanocomposite polymer hydrogels. Colloid and Polymer Science 287, 1-11.
Shao, C., Chang, H., Wang, M., Xu, F., Yang, J., 2017. High-strength, tough, and self-healing nnocomposite physical hydrogels based on the synergistic effects of dynamic hydrogen bond and dual coordination bonds. ACS Applied Materials and Interfaces 9, 28305-28318.

Shen, F., Kang, G., Lam, Y.C., Liu, Y., Zhou, K., 2019. Thermo-elastic-viscoplastic-damage model for self-heating and mechanical behavior of thermoplastic polymers. International Journal of Plasticity 121, 227-243.
Shi, F.K., Wang, X.P., Guo, R.H., Zhong, M., Xie, X.M., 2015. Highly stretchable and super tough nanocomposite physical hydrogels facilitated by the coupling of intermolecular hydrogen bonds and analogous chemical crosslinking of nanoparticles. Journal of Materials Chemistry B 3, 1187-1192.
Su, X., Peng, X., 2018. A 3D finite strain viscoelastic constitutive model for thermally induced shape memory polymers based on energy decomposition. International Journal of Plasticity 110, 166-182.
Sun, J.Y., Zhao, X., Illeperuma, W.R.K., Chaudhuri, O., Oh, K.H., Mooney, D.J., Vlassak, J.J., Suo, Z., 2012. Highly stretchable and tough hydrogels. Nature 489, 133-136.
Thakur, S., Govender, P.P., Mamo, M.A., Tamulevicius, S., Mishra, Y.K., Thakur, V.K., 2017a. Progress in lignin hydrogels and nanocomposites for water purification: Future perspectives. Vacuum 146, 342-355.
Thakur, S., Govender, P.P., Mamo, M.A., Tamulevicius, S., Thakur, V.K., 2017b. Recent progress in gelatin hydrogel nanocomposites for water purification and beyond. Vacuum 146, 396-408.
Vernerey, F.J., Long, R., Brighenti, R., 2017. A statistically-based continuum theory for polymers with transient networks. Journal of the Mechanics and Physics of Solids 107, 1-20.
Vernerey, F.J., 2018. Transient response of nonlinear polymer networks: A kinetic theory. Journal of the Mechanics and Physics of Solids 115, 230-247.
Vernerey, F.J., Brighenti, R., Long, R., Shen, T., 2018. Statistical damage mechanics of polymer networks. Macromolecules 51, 6609-6622.
Wang, Q., Gao, Z., 2016. A constitutive model of nanocomposite hydrogels with nanoparticle crosslinkers. Journal of the Mechanics and Physics of Solids 94, 127-147.
Wang, Q., Gao, Z., Yu, K., 2017. Interfacial self-healing of nanocomposite hydrogels: Theory and experiment. Journal of the Mechanics and Physics of Solids 109, 288-306.
Xiang, Y., Zhong, D., Wang, P., Yin, T., Zhou, H., Yu, H., Baliga, C., Qu, S., Yang, W., 2019. A physically based visco-hyperelastic constitutive model for soft materials. Journal of the Mechanics and Physics of Solids 128, 208-218.
Xiao, R., Mai, T.T., Urayama, K., Gong, J.P., Qu, S., 2021. Micromechanical modeling of the multi-axial deformation behavior in double network hydrogels. International Journal of Plasticity 137, 102901.
Xu, C., Dai, G., Hong, Y., 2019. Recent advances in high-strength and elastic hydrogels for 3D printing in biomedical applications. Acta Biomaterialia 5, 50-59.
Yang, Q., Li, G., 2016. Temperature and rate dependent thermomechanical modeling of shape memory polymers with physics based phase evolution law. International Journal of Plasticity 80, 168-186.
Yang, B., Yao, F., Hao, T., Fang, W., Ye, L., Zhang, Y., Wang, Y., Li, J., Wang, C., 2016. Development of electrically conductive double-network hydrogels via one-step facile strategy for cardiac tissue engineering. Advanced Healthcare Materials 5, 474-488.
Yin, H.M., Sun, L.Z., Chen, J.S., 2002. Micromechanics-based hyperelastic constitutive modeling of magnetostrictive particle-filled elastomers. Mechanics of Materials 34, 505-516.
Yu, K., Xin, A., Wang, Q., 2018. Mechanics of self-healing polymer networks crosslinked by dynamic bonds. Journal of the Mechanics and Physics of Solids 121, 409-431
Zaïri, F., Gloaguen, J.M., Naït-Abdelaziz, M., Mesbah, A., Lefebvre, J.M., 2011. Study of the effect of size and clay structural parameters on the yield and post-yield response of

polymer/clay nanocomposites via a multiscale micromechanical modelling. Acta Materialia 59, 3851-3863.
Zhai, X., Ma, Y., Hou, C., Gao, F., Zhang, Y., Ruan, C., Pan, H., Lu, W.W., Liu, W., 2017. 3D-printed high strength bioactive supramolecular polymer/clay nanocomposite hydrogel scaffold for bone regeneration. ACS Biomaterials Science and Engineering 3, 1109-1118.
Zhang, W., Feng, P., Chen, J., Sun, Z., Zhao, B., 2019. Electrically conductive hydrogels for flexible energy storage systems. Progress in Polymer Science 88, 220-240.
Zhou, J., Jiang, L., Khayat, R.E., 2018. A micro-macro constitutive model for finite-deformation viscoelasticity of elastomers with nonlinear viscosity. Journal of the Mechanics and Physics of Solids 110, 137-154.
Zhu, P., Zhong, Z., 2020. Modelling the mechanical behaviors of double-network hydrogels. International Journal of Solids and Structures 193-194, 492-501.

Parameter	Significance	Matrix-1	Matrix-2	Hydrogel-based nanocomposites (ϕ = 10%)				
				ZIF-8	ZIF-67	UiO-66	SiO_2	Fe^{3+}
N	Mean chain length	30	10	47	35	22	30	3
n (m^{-3})	Mean chain density	1.05×10^{27}	1.34×10^{26}	1.46×10^{27}	1.46×10^{27}	2.36×10^{27}	8.26×10^{27}	2.19×10^{27}
ν_m	Matrix Poisson's ratio	0.49	0.49	0.49	0.49	0.49	0.49	0.49
$\mu_p/\mu_m = K_p/K_m$	Moduli mismatch	0	0	60	60	60	30	50
k_{on/off_0} (s^{-1})	Dynamic bonds	5×10^{-5}	5×10^{-5}	5×10^{-5}	5×10^{-5}	5×10^{-5}	5×10^{-5}	5×10^{-5}
σ_{off} (MPa)	Bonds strength	12	0.69	150	165	150	380	Eq. (35)
k_{v_0} (MPa^{-1} s^{-1})	Viscous multiplier	6×10^{-5}	1.24×10^{-4}	1.087×10^{-4}	1.087×10^{-4}	1.087×10^{-4}	8.7×10^{-5}	Eq. (36)
$\dot{\lambda}_0$	Reference loading rate	0.01	0.01	0.01	0.01	0.01	0.01	0.01
τ	Rate-dependency	0.8	0.8	0.8	0.8	0.8	0.8	0.8
α	Stretch-dependency	1.2	1.8	2.1	2.1	2.1	0.9	0.69

Table 1. Model parameters for various hydrogel-based systems with cross-linker amount of 1 mg.

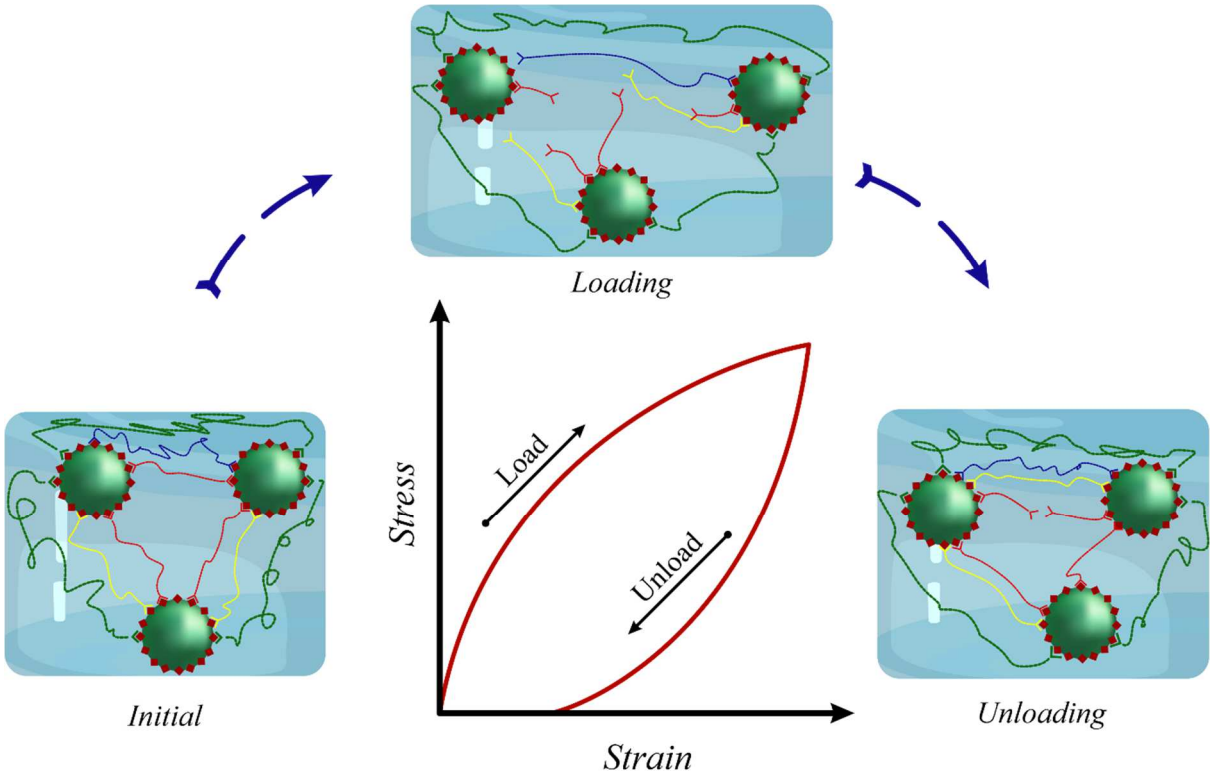

Figure 1. Dynamic bonds in hydrogel-filler material system upon a stretching-retraction cycle. Each color is associated to a group of chains according to their lengths.

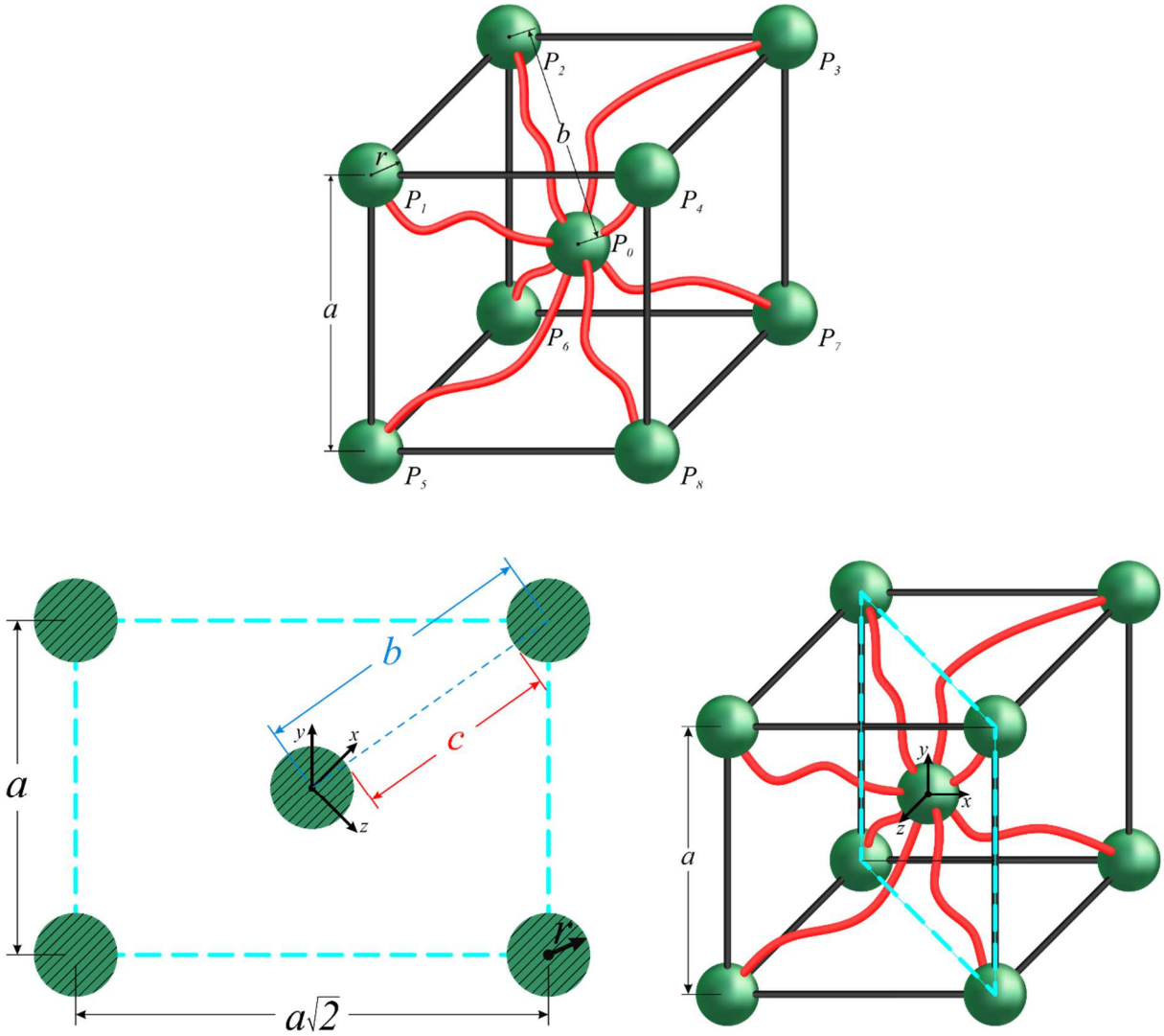

Figure 2. Unit cell and corresponding geometric setting.

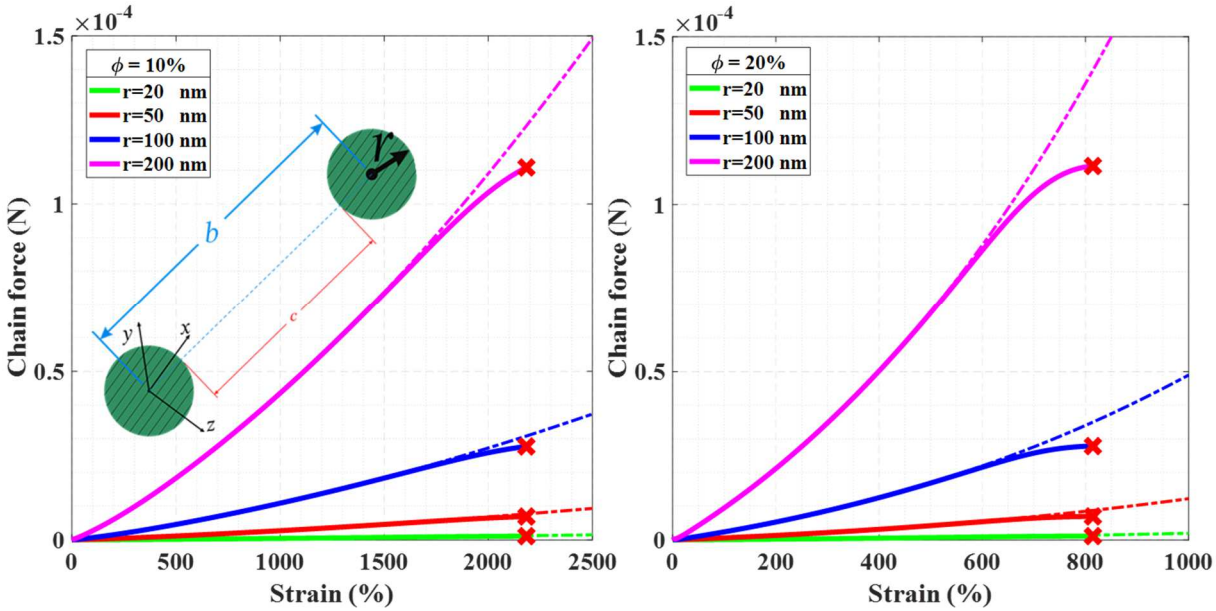

(a) (b)

Figure 3. Model results for the chain force evolution at different particle radii considering a purely elastic response (dashed lines) and detachment mechanism (solid lines): (a) 10% filler amount, (b) 20% filler amount.

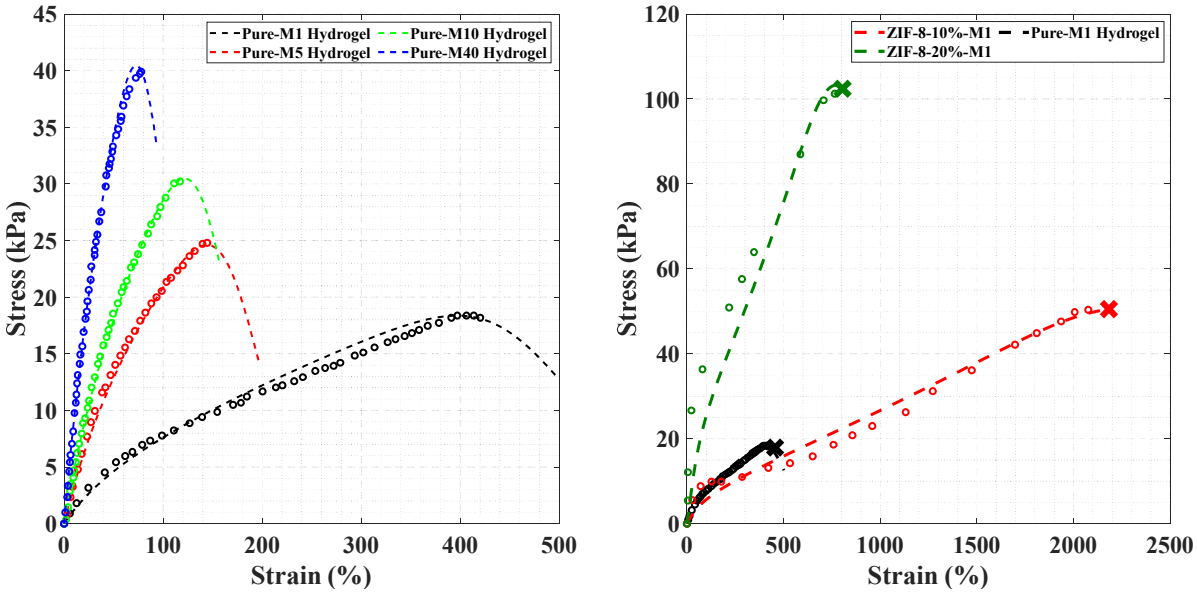

(a) (b)

Figure 4. Stress-strain curves of the pure hydrogel and the hydrogel-based nanocomposites: (a) pure hydrogel for different cross-linker amounts, (b) hydrogel-ZIF-8 systems for different filler amounts (lines: model calibration results, symbols: experiments).

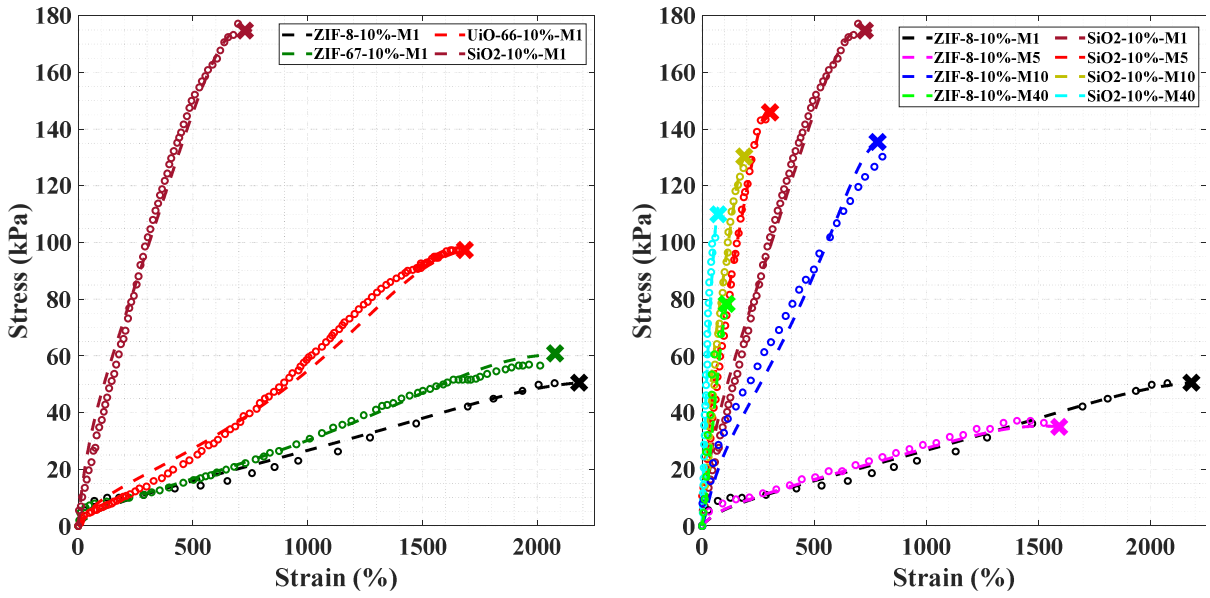

(a) (b)

Figure 5. Stress-strain curves of the hydrogel-based nanocomposites for different filler types: (a) ZIF-8, ZIF-67, UiO-66 and SiO2 (b) ZIF-8 and SiO_2 for different cross-linker amounts (lines: model calibration results, symbols: experiments).

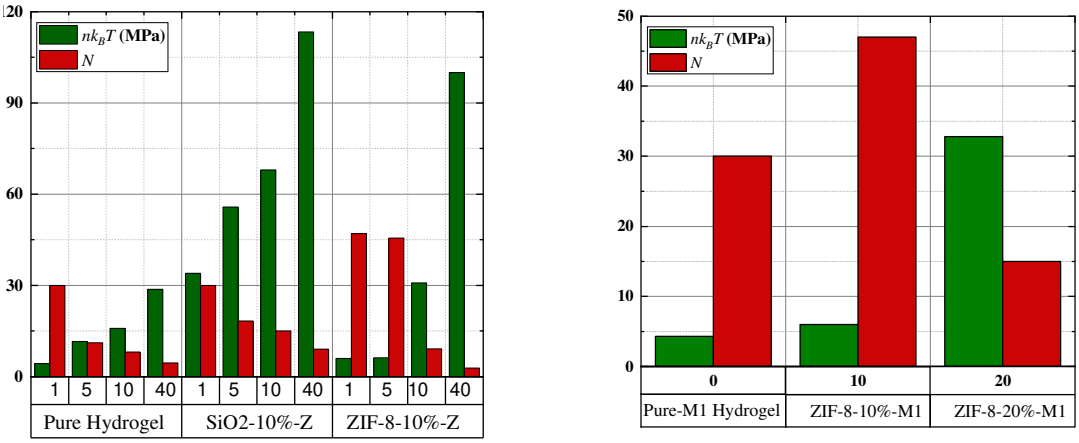

(a) (b)

Figure 6. Mean chain density n and mean chain length N: (a) Effect of the cross-linker amount (in mg with Z = 1, 5, 10 and 40), (b) effect of the filler amount (in %).

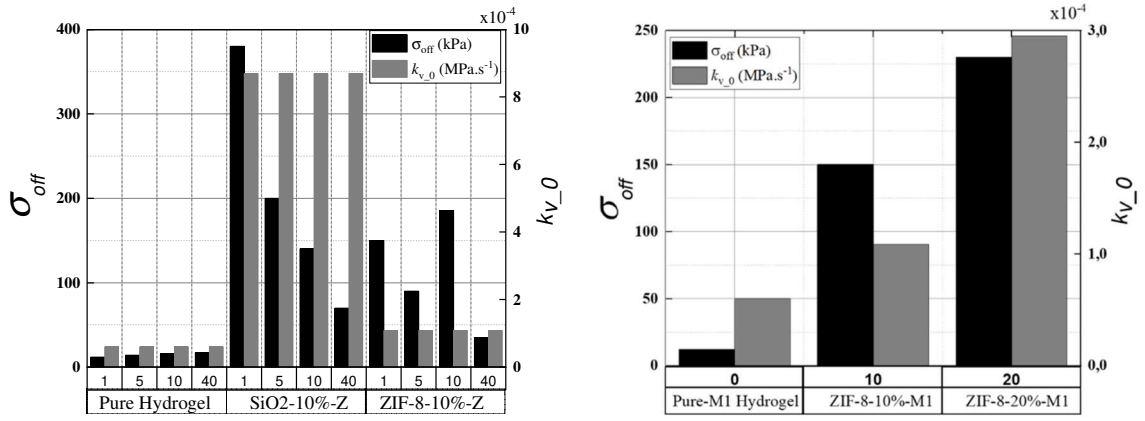

(a) (b)

Figure 7. Bonds strength σ_{off} and chains viscosity k_{v_0}: (a) Effect of the cross-linker amount (in mg with Z = 1, 5, 10 and 40), (b) effect of the filler amount (in %).

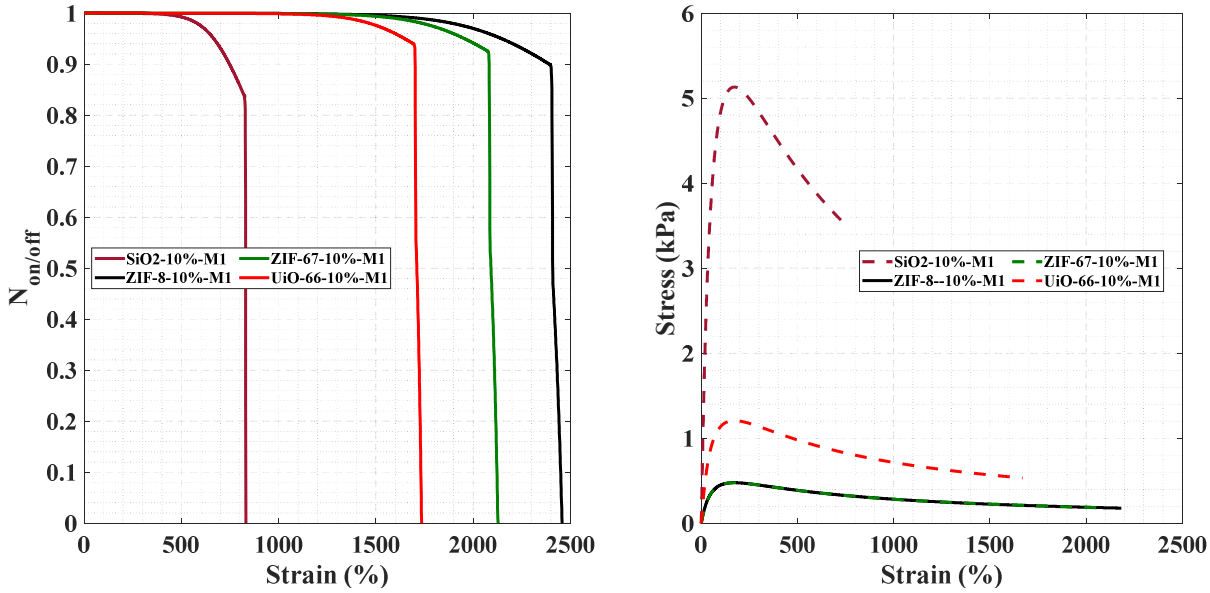

(a) (b)

Figure 8. Evolution as a function of strain of (a) chains network translated by $N_{on/off}$ and (b) stress in nanoparticles for different filler types.

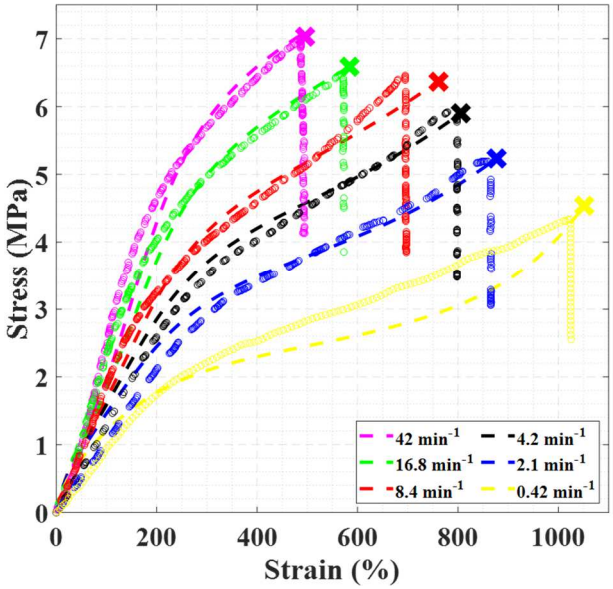

Figure 9. Stress-strain curves of the hydrogel-based Fe^{3+} nanocomposites for different stretch rates (lines: model calibration results, symbols: experiments).

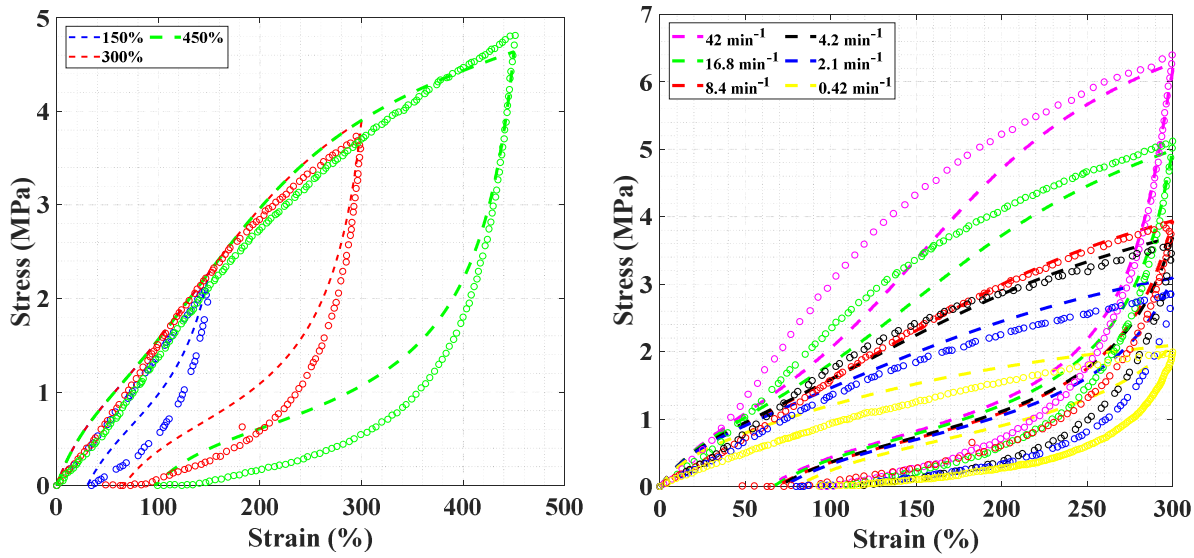

(a) (b)

Figure 10. Stress-strain curves of the hydrogel-based Fe^{3+} nanocomposites upon a stretching-retraction cycle at (a) a stretch rate of 8.4 min^{-1} and at different stretch levels, (b) different stretch rates and a strain level of 300% (lines: model, symbols: experiments).

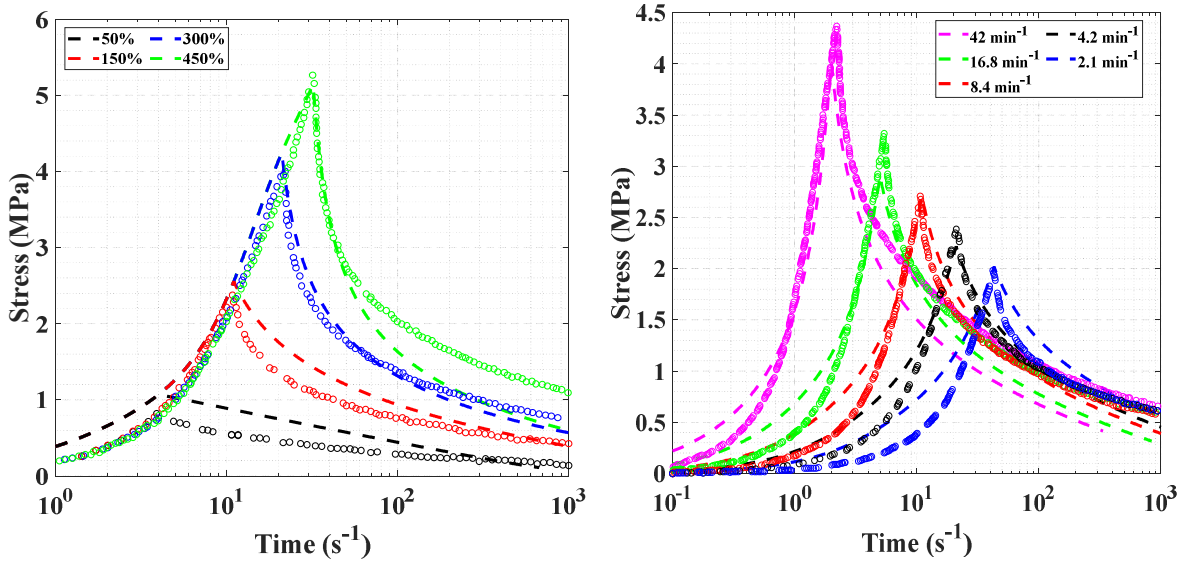

(a) (b)

Figure 11. Temporal stress changes of the hydrogel-based Fe^{3+} nanocomposites upon a stretching followed by a relaxation at (a) different strain levels and a stretch rate of 8.4 min^{-1}, (b) a strain level of 150% and different stretch rates (lines: model, symbols: experiments).

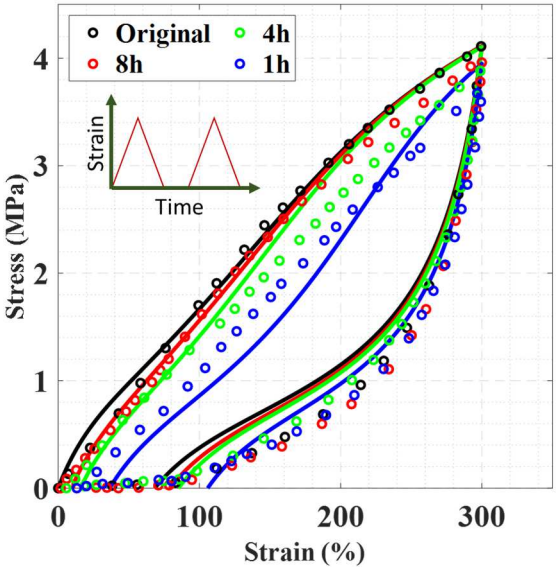

Figure 12. Recovery time effect on the second stretching-retraction cycles of the hydrogel-based Fe^{3+} nanocomposites at a stretch rate of 8.4 min^{-1} and a strain level of 300% (lines: model, symbols: experiments).

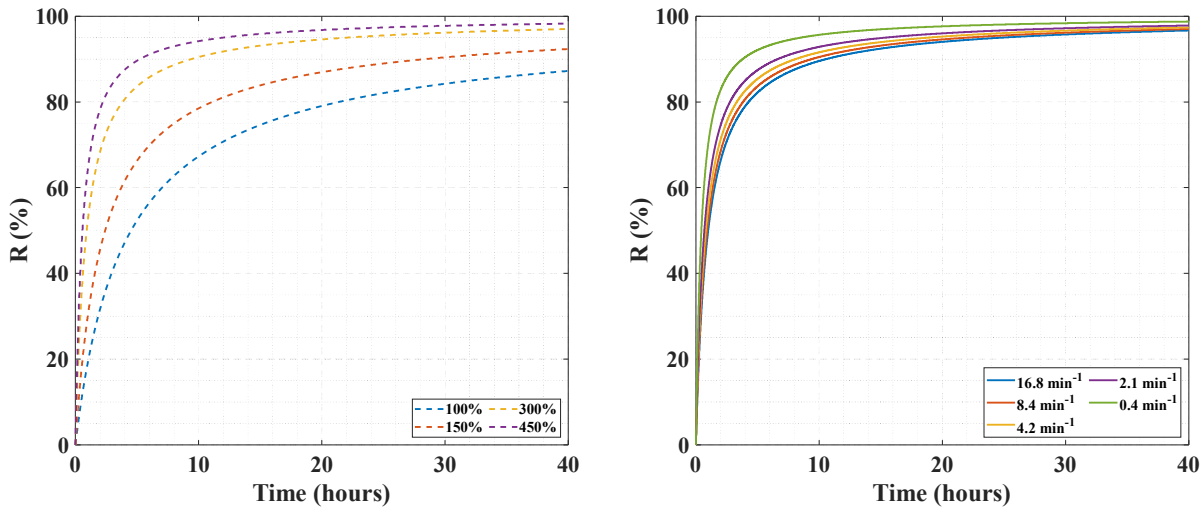

(a) (b)

Figure 13. Recovery behavior of the hydrogel-based Fe^{3+} nanocomposites previously stretched at (a) different stretch levels at a stretch rate of 8.4 min^{-1}, (b) different stretch rates at a strain level of 300%.

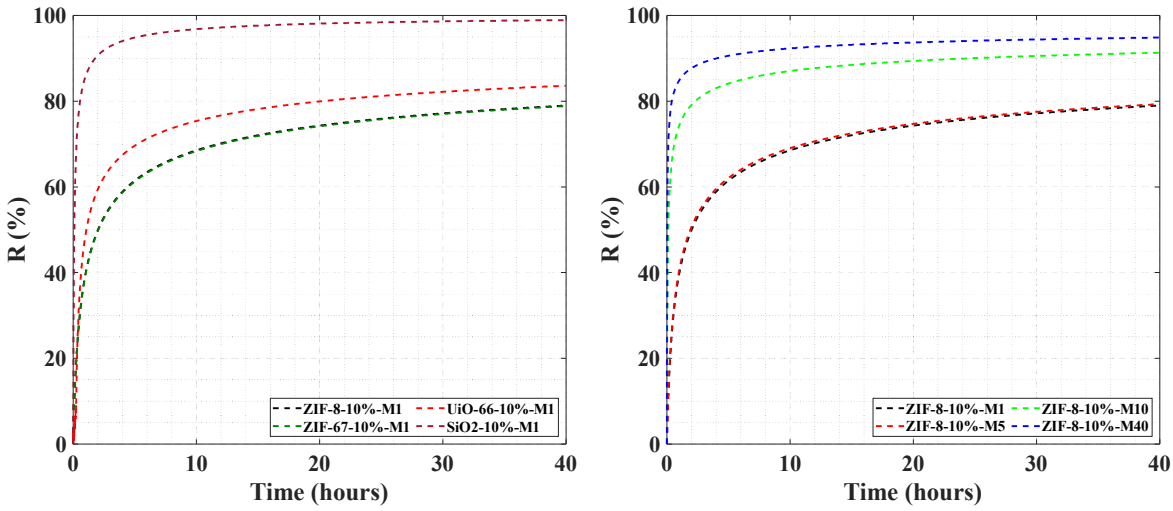

(a) (b)

Figure 14. Recovery behavior of the hydrogel-based nanocomposites previously stretched at a stretch rate of 30 min^{-1} and a strain level of 300%: (a) different filler types, (b) different cross-linker amounts.

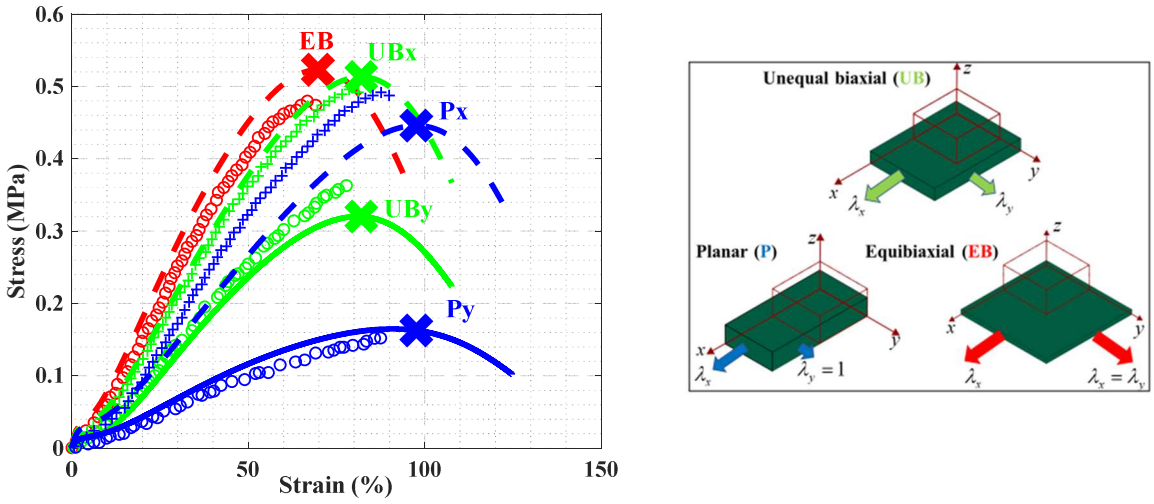

Figure 15. Stress-strain curves of the pure hydrogel under different biaxial loading conditions (lines: model, symbols: experiments).

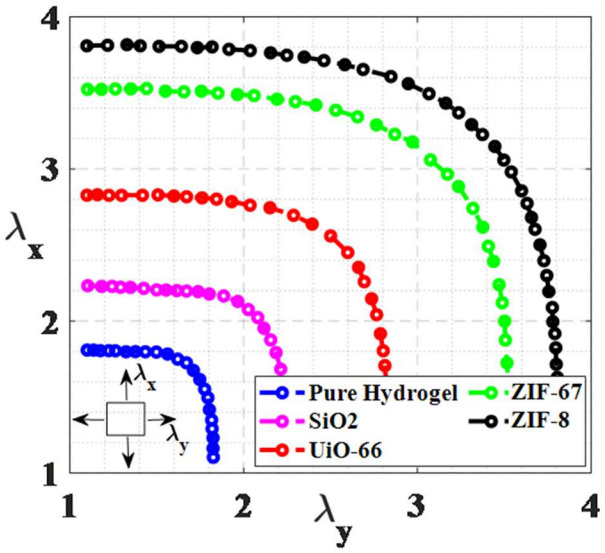

Figure 16. Model results for the biaxial failure envelope of the pure hydrogel and the hydrogel-based nanocomposites (with cross-linker amount of 1 mg and filler amount of 10%).